RAMAN APPLICATIONS IN NANODIAGNOSTICS AND TEMPLATING

A Thesis

submitted in partial fulfillment for the degree of

Master of Science

as part of the

Integrated Ph.D programme

(Materials Science)

By

SOUMIK SIDDHANTA

CHEMISTRY AND PHYSICS OF MATERIALS UNIT

JAWAHARLAL NEHRU CENTRE FOR ADVANCED SCIENTIFIC RESEARCH

BANGALORE – 560 064, INDIA.

MAY 2010

DECLARATION

I hereby declare that the matter embodied in this thesis entitled "**Raman Applications in Nanodiagnostics and Templating**" is the result of the investigations carried out by me in the Chemistry and Physics of Materials Unit, Jawaharlal Nehru Centre for Advanced Scientific Research (JNCASR), Bangalore, India, under the supervision of Professor Chandrabhas Narayana.

In keeping with the general practice of reporting scientific observations, due acknowledgements have been made whenever the work described is based on the findings of other investigators. Any omission which might have occurred by oversight or error in judgement is regretted.

_____

(Soumik Siddhanta)

CERTIFICATE

I hereby certify that the matter embodied in this thesis entitled "**Raman Applications in Nanodiagniostics and Templating**" has been carried out by Mr. Soumik Siddhanta at the Chemistry and Physics of Materials Unit, Jawaharlal Nehru Centre for Advanced Scientific Research (JNCASR), Bangalore, India under my supervision and that it has not been submitted elsewhere for the award of any degree or diploma.

_____

Prof. Chandrabhas Narayana

(Research Supervisor)

Acknowledgements

Firstly I would like to thank my supervisor Prof. Chandrabhas Narayana for his continuous guidance and support. He was always there to listen and give advice. His positive attitude and enthusiasm is a source of great inspiration to me. I would like to thank him for his excellent guidance and hope that I will be able to become a good scientist and a good human being.

I would like to thank Prof. C.N.R. Rao for being a source of great inspiration. His enthusiasm towards science is something for me to cherish forever.

I would like to thank Prof. Sampath (IISc Bangalore), Prof. K.N. Ganesh (IISER, Pune), Dr. K.V. Ramana (DFRL, Mysore), Dr. Uday K. Ranga (JNCASR, Bangalore), Dr. E. Prabhakaran (IISc, Bangalore), Mr. Chandramouli and Mr. Sudip Mohapatra (JNCASR), Tirupathi (IISc, Bangalore). Discussing scientific ideas with them was a great learning experience for me.

I would also like to thank my past and present labmates Gopal, Pavan, Kavitha, Diptikanta, Nashiour, Navneet, Partha, Srinu, Gayatri, Ritu, Gayatri Nair and Sonia. I really enjoyed working alongside them and also the lab trips and parties. Special thanks to Gopal for being a source of great help and enthusiasm.

I am thankful to the faculty members and staff of JNC. I would like to thank Prof. Ranganathan (IISc, Bangalore), Prof. Balasubramanian, Prof. G.U. Kulkarni, Prof. Sundaresan, Prof. Easwaramoorthy, Prof. K.S. Narayan, Prof. Tapas Maji, Dr. Subi George, Dr. T. Govindaraju, Dr. Vidyadhiraja, Prof. Shobhana Narasimhan, Prof.

Swapan Pati, Prof. Umesh Waghmare, Prof. S.M. Shivaprasad and Mrs. Sobha of JNCASR for their teaching during course work which were extremely beneficial for me.

I would like to thank Usha Madam, Vasu, Basavraj and Selvi for their help with characterization techniques. I thank all the academic, technical, library and complab staff at JNCASR.

I am privileged to have wonderful batchmates Ritu, Abhay, Bivas, Nisha, Nitesh, Vini, Piyush, Urmi and Shekhar. I am also grateful to have fantastic seniors and juniors of Int. PhD.

I would also like to thank all my friends at JNC who have made my stay at JNC pleasurable.

I would also like to thank my college teachers Dr. R.K. Trikha and Dr. Nayyar and also my wonderful school and college teachers for their encouragement and blessings

I thank my family members for their encouragement, support and love.

Preface

A lot of techniques for detection of specific Nucleic acid sequences have been used for diagnosis of diseases. Some of the techniques involve labeling oligonucleotides with specific sequences with fluorescence dyes and use hybridization for detection of the required base sequences. Expensive techniques like PCR are also used to detect nucleic acids at real time. The high cost and technical skills required for PCR technique and complex chemistry involved in fluorescent labeling are the drawbacks of these processes.

A novel technique involving core shell super-paramagnetic nanoparticles, oligonucleotide capture and detector probes have been devised for easy separation and detection of specific sequences of nucleotides. The detector probes hybridized to specific base sequences and labeled with Raman probes are detected by using Surface Enhanced Raman Spectroscopy which is a highly sensitive and versatile technique. The level of detection of analyte molecule can go down to ultralow concentration levels and even to single molecular level.

One of the several significant usages of graphene and graphite oxide as well as carbon nanotubes is that of chemical sensors. The characteristics and concentration of defects on graphene gives rise to interesting properties which can be harnessed to make molecular and gas sensors. Raman spectroscopy studies of defects on graphite oxide on interaction with small molecules have shown that this method can be optimized and possibly can be used as sensors for small biologically relevant molecules like amino acids and glucose.

The preparation of nanomaterials which gives optimum and quantitative SERS is a challenging area of research now. Nanostructures of various shapes, sizes and arrangements are made these days which are being tested for their efficiency in giving good SERS signals with high enhancement factors. Multifunctional silver nanorods synthesized were found to give good enhancement factor to be used in SERS studies. Also methods of encapsulation of gold nanoparticles inside organic microtubes to form nanoarrays of gold nanoparticles have been devised. This method can be used like lithography to pattern nanoparticles or form arrays at desired locations. These nanoparticle arrays are also SERS active. Therefore they can be used for trace molecules detection.

Templating biomaterials for growth of nanostructures have also gained considerable interest owing to their multifunctionality. These materials being environment friendly, cost effective and being easily available are attractive materials to be used in a variety of applications from antibacterial wound dressing materials to building substrates for ultrasensitive chemical and biochemical analysis.

Bacterial cellulose, naturally occurring polymers, have considerable mechanical strength and porosity to be used as an antibacterial material. Its efficiency can be further improved by incorporating silver nanoparticles which has proven antibacterial activity. Not only silver nanoparticle incorporation makes it a better antibacterial material but also these plasmonic nanoparticles can be utilized for SERS for ultra-trace analysis making these materials truly multifunctional. A simple method has been used to incorporate silver chloride and silver nanoparticles into bacterial cellulose for its use as antibacterial materials and also template for SERS.

In this thesis, Chapter 1 contains introduction to the topics. Chapter 2 deals with Nucleic acid detection by SERS using oligonucleotide capped core shell nanoparticles. Chapter 3 deals with the Graphite oxide as molecular sensors. Chapter 4 deals with formation of nanoparticle arrays and multifunctional nanostructures for Surface Enhanced Raman Spectroscopy. Chapter 5 deals with Incorporation of silver chloride and silver nanoparticles in bacterial cellulose membranes.

Table of Contents

Chapter 1

Introduction

The rapid development in spectroscopic techniques has revolutionized our understanding of molecular structure, detection as well as molecular interactions. Vibrational spectroscopy is one of the oldest and classical techniques of spectroscopy. The beginning of the last century has seen the use of IR radiation to produce the first vibrational spectra. In 1920's the discovery of Raman effect[1] by Chandrashekhara V. Raman opened up an area of new type of vibrational spectroscopy. Raman spectroscopy was further developed by the development of lasers by Maiman in 1960, the introduction of double and triple monochromators and most importantly Charge Coupled Devices or CCD's. The sensitivity and effectiveness of these techniques have made them indispensable in wide range of areas, from pharmaceuticals to semiconductor industries. Nowadays Raman spectroscopy is used to study a wide range of materials and diverse systems. With the advent of commercially available lasers and high resolution spectrometers Raman spectroscopy was introduced in the field of biology to study complex biomolecules.

Raman coupled with IR spectroscopy started a whole new area of interdisciplinary research comprising of the interface of physics, chemistry and biology. Vibrational spectroscopy offers many advantages. Details of molecular structure and molecular interactions can be elucidated with a resolution greater than highly resolved crystal

structures. The size of sample does not matter, thus information can be extracted from small molecules to complex biological systems[2]. The molecules can be studied in a variety of environments and state, for example in solid, liquid or in monolayers according to specific requirements. Combining these techniques with time resolved approaches gives detailed information about the dynamics of molecules down to femtosecond time scale. The application of classical Raman scattering has many drawbacks like low scattering cross sections and sample fluorescence which reduces its efficiency to a great extent. To counteract these problems new techniques were developed like Resonance Raman spectroscopy, Surface Enhanced Raman Spectroscopy, non-linear coherent Raman spectroscopy etc. These improved techniques have helped in their implementation in highly sensitive experiments like single molecule detection, observation of modes forbidden in both Raman and IR spectroscopy and also suppression of fluorescence leading to increase in signal strength. Infrared and Raman spectroscopy are the two most commonly used techniques to study the vibrational spectra of the molecules which are considered to be their fingerprints. The present work mostly deals with Raman scattering techniques like Raman spectroscopy and Surface enhanced Raman Spectroscopy to study different systems.

1.1 Raman scattering

When a light quantum $h\upsilon_0$ hits a molecule an elastic scattering called Raleigh scattering happens with quanta energy of $h\nu_0$ [3]. The inelastic process which consists of exchange of vibrational energy and with a lower probability is called Raman scattering. It emits quanta of energy $h\nu_0 \pm h\nu_s$. At ambient temperature most molecules are in their vibrational ground state and very few are in their vibrational excited state according to the Boltzmann's law. Therefore the Raman process which transfers vibrational energy to the molecule and leaves with a lower energy of $h\nu_0 - h\nu_s$ has a higher probability than the other process. Stokes lines are the ones caused by quanta of lower energy and those by higher energy are called anti stokes. Stokes lines are generally recorded in the Raman spectra as their intensities are greater than the anti stokes lines. Coming to molecular vibrations each atom has three degrees of freedom along each axes of the cartesian coordinate. If n atoms constitute a molecule there are $3n$ degrees of motional freedom. Three are translational parallel to the three cartesian axes and the other three are rotational about the principal axes of the inertial ellipsoid of the molecule. The remaining $3n-6$ degrees are motions which change the distances between the atoms, the lengths of chemical bonds and the angle between them. If bond vibrations can be compared to a harmonic oscillator, then according to classical mechanics it may vibrate with any amplitude or it may possess any amount of energy. Quantum mechanics however shows

that molecules can only exist in definite energy states. In case of harmonic potentials these states are equidistant,

$$E_i = h\nu(\nu_i + \frac{1}{2}) \quad \text{where } \nu_i = 0,1,2,3\ldots$$

while for anharmonic potentials the distances between energy levels decreases with increasing energy. These energy levels are numbered ν_i, the vibrational quantum number. The molecular potentials are not exactly harmonic but the harmonic approximation is satisfactory. Classical mechanics can describe molecular vibration frequencies but it is quantum mechanics which can specify the change of energy of the vibrational states and the interaction with the light quanta which are absorbed, emitted or scattered by a molecule. When a molecule is exposed to an electric field, electrons and nuclei are forced to move in opposite directions. A dipole moment is induced which is proportional to the electric field strength and to the molecular polarizability α. A molecular vibration can be observed in Raman spectra if there is a modulation of the molecular polarizability by the vibration.

$$\left(\frac{\partial \mu}{\partial q}\right)_O \neq 0 \quad ,$$

where μ is the molecular dipole moment and q stands for the normal coordinate describing the motion of the atoms during a normal vibration. If this condition is satisfied then the vibration is said to be Raman active. The absolute intensity of a line provides

information about the molecular structure. It shows the modulation of the molecular polarizability by a vibration. If a molecule is placed under a static electric field the induced dipole moment of a molecule depends upon the applied electric field and is given by[4]

$$p = \alpha.E$$

where α is the polarizability of the molecule. Since p and E are three dimensional vectors, α can be written as a tensor whose components can be represented as elements of a matrix.

$$\begin{bmatrix} P_x \\ P_y \\ P_z \end{bmatrix} = \begin{bmatrix} \alpha_{xx} & \alpha_{xy} & \alpha_{xz} \\ \alpha_{yx} & \alpha_{yy} & \alpha_{yz} \\ \alpha_{zx} & \alpha_{zy} & \alpha_{zz} \end{bmatrix} \begin{bmatrix} E_x \\ E_y \\ E_z \end{bmatrix}$$

If the molecules are subjected to electromagnetic radiation of frequency ν which has an oscillatory field given by

$$E = E_o \sin 2\pi\nu t$$

The oscillatory induced dipole moment is given by

$$p = \alpha.E = \alpha E_o \sin 2\pi\nu t$$

The oscillation in dipole moment leads to Rayleigh scattering which is the elastic scattering component.

If the molecules have internal degrees of freedom like vibration or rotation which changes the polarizability periodically, then the oscillating dipole is a superposition of varying electric field and polarizability. In such a case, polarizability is given by

$$\alpha = \alpha_o + \beta \sin 2\pi\nu t$$

where α_0 is the equilibrium polarizability, β is the rate of change of polarizability and ν_{vib} is the vibrational frequency of the molecule. Then the induced dipole moment is given by

$$p = \alpha E_o \sin 2\pi\nu t + \beta E_o \left\{\cos 2\pi(\nu - \nu_{vib}) - \cos 2\pi(\nu + \nu_{vib})\right\}$$

The components $\nu - \nu_{vib}$ and $\nu + \nu_{vib}$ are called stokes and anti stokes lines respectively. Therefore for a vibrational mode to be Raman active $\beta \neq 0$, that is there must be a change in component of molecular polarizability. As mentioned above in the quantum picture the molecules exist in quantized energy levels corresponding to possible stationary states of the molecule. In case of IR absorption there is a direct transition between vibrational energy levels. But in case of Rayleigh and Raman scattering transitions proceed via the virtual states which does not correspond to an eigen state of the molecule.

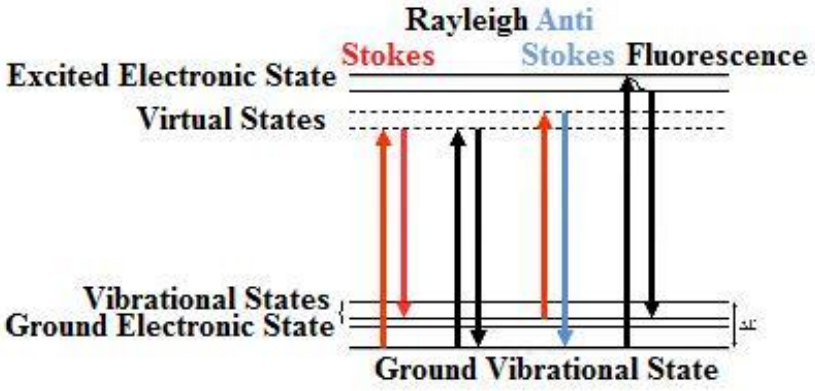

Figure 1.1 Energy level diagram comparing Raman and fluorescence

The amplitude of a transition from an initial state i to a final state f induced by radiation of wavenumber ν_0 is given as

$$[\mu]_{f_i} = \langle \psi_f | \alpha | \psi_i \rangle . E$$

where ψ_i and ψ_f are wavefunctions of initial and final states.

The typical matrix element of the transition polarizability associated with stokes Raman scattering at Raman shift is given by

$$\left[\alpha_{xy}\right] = b\beta\sqrt{v+1}$$

$$b = \frac{\hbar}{4\pi c v}$$

where v is the vibrational quantum number and b is the quantum mechanical analog of the amplitude of a classical oscillator. At least one component of the derived polarizability tensor has to be nonzero for the transition to be Raman active.

Considering scattering from N molecules, the ratio of intensities with respect to stokes and anti stokes like is given by

$$\frac{I_{Stokes}}{I_{anti-stokes}} = \left(\frac{\nu_0 - \nu_k}{\nu_0 + \nu_k}\right)^4 \exp\left(\frac{hc\nu}{kT}\right)$$

This equation is also used to find the sample temperature.

The expression for Raman cross section is given as

$$\sigma(i \to f) = \frac{8\pi\omega_s{}^4}{9\hbar c^4}\left|\sum_j \frac{\langle\alpha_{ij}\rangle\hat{e}_L\langle\alpha_{jf}\rangle\hat{e}_s}{\omega_{ij} - \omega_L - i\gamma_L} + \frac{\langle\alpha_{ji}\rangle\hat{e}_L\langle\alpha_{jf}\rangle\hat{e}_s}{\omega_{jf} - \omega_L - i\gamma_j}\right|^4$$

the sum extends over all molecular levels j with homogeneous width γ, accessible by single photon transitions from the initial state. The scattering cross section of a molecule can be increased by a few orders of magnitude when Raman excitation frequency is in resonance with one of the electronic transitions of the molecule. This effect is known as Resonant Raman scattering. Figure 1.1 shows the energy level diagram comparing Raman and fluorescence.

1.2 Surface Enhanced Raman Scattering

To use Raman scattering as a spectroscopic technique has several drawbacks. About one in 10^8 photons undergo Raman scattering, therefore the Raman signal is very low from low concentrations of analyte or from poor Raman scatterers. Sometimes the high fluorescence from the molecule obscures the Raman signals. Surface Enhanced Raman Spectroscopy is a technique where molecules undergo much higher scattering efficiencies when adsorbed on metal colloidal nanoparticles or rough metal surface. First observed by Fleischman[5] *et. al.* in 1974 and discovered by Jeanmarie and Van Duyne[6] and Albrecht and Creighton in 1977[7], SERS is now being increasingly used to study organic and biomolecules.

1.2.1 Electromagnetic Mechanism of SERS

Light incident on metal nanoparticles or rough surfaces can excite conduction electrons in the metal generating collective oscillations of free electrons on the metal surface. This is called surface plasmon[8]. The particle becomes polarized and the electric field in the interior of the particle becomes significantly larger than the applied field and falls off as $1/r^3$ away from the surface. When the exciting laser light is resonant with the dipolar plasmon the metal nanoparticle will radiate light characteristic of dipolar radiation. Light intensity from certain portions of space surrounding the particle is depleted while the intensity at certain portions near the metal is enhanced. Any molecule

near the particle will be influenced by this strong electric field. Lets consider a small sphere with complex dielectric constant $\varepsilon(\nu)$ in a surrounding medium with a dielectric constant $\varepsilon(0)$. The diameter of the sphere is $2r$ and is smaller than the wavelength of light. A molecule which is at a distance d from the nanoparticle is exposed to an electric field E_m, which is a superposition of the incoming field and the dipole field induced in the metal sphere.

The expression for field enhancement factor is given as:

$$A(\nu) = \frac{E_m(\nu)}{E(\nu)} = \frac{\varepsilon - \varepsilon_o}{\varepsilon + 2\varepsilon_o}\left(\frac{r}{r+d}\right)^3$$

The value of $A(\nu)$ is large when the real part of ε is equal to $-2\varepsilon_0$.

For a strong electromagnetic enhancement, the imaginary part of the dielectric constant should be small. Metals like Ag, Au, Cu satisfy this consition at visible wavelengths and therefore exhibit strong SERS. The Stokes or anti-Stokes field is enhanced if it is in resonance with the surface plasmons of the metal spheres. The electromagnetic enhancement factor for the Stokes scattering is given by

$$G_{em}(\nu s) = \left|A(\nu_L)\right|^2 \left|A(\nu_s)\right|^2 = \left|\frac{\varepsilon(\nu_L) - \varepsilon_o}{\varepsilon(\nu_L) + 2\varepsilon_o}\right|^2 \left|\frac{\varepsilon(\nu_s) - \varepsilon_o}{\varepsilon(\nu s) + 2\varepsilon_o}\right|^2 \left(\frac{r}{r+d}\right)^{12}$$

The enhancement scales as fourth power of the local field at the vicinity of the metallic nanostructure and is strong when the scattered and the plasmon field are in resonance. This enhancement is distance dependent and decays as $(r/(r+d))^{12}$. Electromagnetic enhancement is stronger than any other enhancements. Contours of the local field near silver particles at specified wavelengths are shown in Figure 1.2.

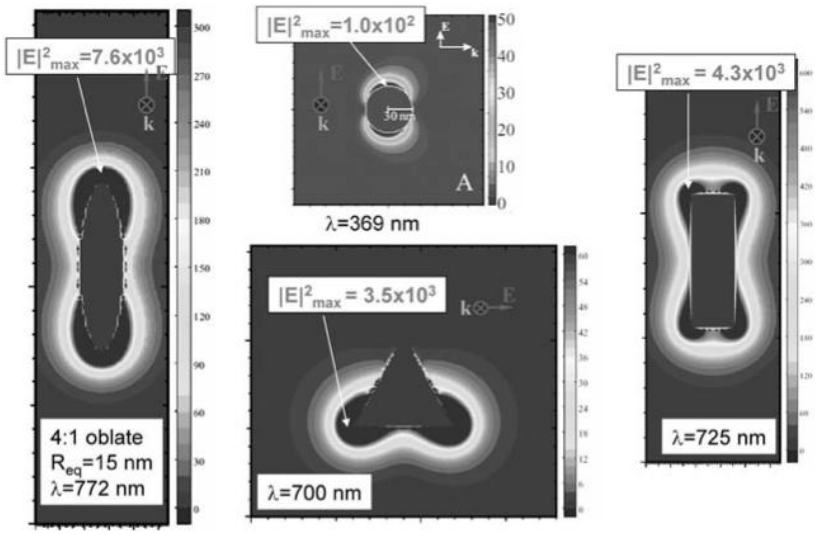

Figure 1.2 Contours of the local field near silver particles at specified wavelengths.

1.2.2 Chemical Enhancement

Chemical enhancement takes place when the molecule is in contact with the metal surface. Molecules may be chemically adsorbed on the nanoparticles with charge transfer excitation. The charge transfer phenomena involve the transfer of an electron from the

Fermi level of the metal to an unoccupied molecular orbital of the adsorbate or vice versa. Resonance Raman scattering also happens because of the charge transfer in the metal complex formed with the adsorbed molecule. Another mechanism of chemical enhancement is the metal-molecule or molecule-metal charge transfer. Charge transfer transition between the Fermi level of the metal nanostructure and the LUMO of the adsorbed molecule happens by the Laser excitation. As shown in Figure, the fermi level is between the HOMO and the LUMO energies of the adsorbate. The molecule must be chemisorbed on to the surface for charge transfer to take place. The laser frequency should be in resonance with the plasmon adsorption of the surface nanostructures giving rise to Surface Enhanced Resonance Raman Spectra. In this process, photon is adsorbed by the metal which results in a hot electron state. This electron gets transferred to the LUMO of the molecule. This hot electron is transferred from LUMO back to the metal. Then the electron returns to its initial state by emitting Stokes photons. Charge transfer excitations between the metal and adsorbed molecules give rise to an enhancement of ~ 10^2.

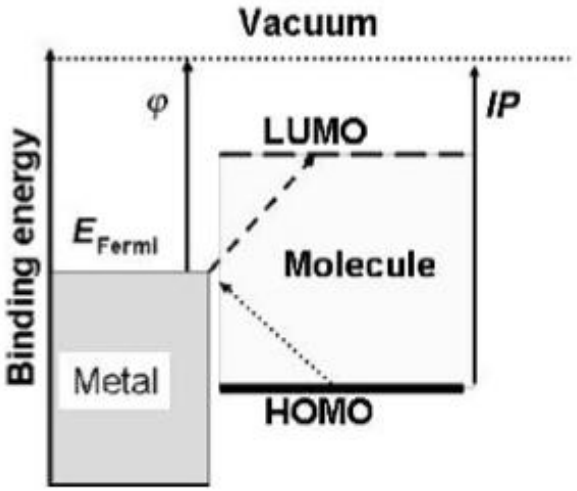

Figure 1.3 Energy diagram illustration the band energy of the metal nanostructure and the HOMO-LUMO gap of the adsorbed molecule

1.3 SERS in Biodiagnostic applications

Detection of nucleic acid sequences and their extraction at ultra low concentrations have become a matter of great interest in the field of material science and spectroscopy. Nucleic acids like DNA and RNA are carriers of genetic information and any disorder in base sequences can cause diseases[9]. Detection of nucleic acids has potential uses in clinical diagnosis, biomedical engineering, forensic biology and biological systematics[10, 11].

Generally scintillation counting, fluorescence, amplification by enzymes and electrochemistry are more commonly used techniques for biomolecules detection[12-15]. But the recent advancement in Raman spectroscopy based techniques like SERS or

SERRS have made it a sensitive tool for biodetection[16, 17]. Recently SERS with the use of metal nanoparticles can be used for single molecule detection[18, 19]. The observed enhancement of 10^{11}-10^{14} have made SERS a major competitor for fluorescence techniques[20, 21].

In a rapidly growing field of molecular diagnostics there is a need for a quick, robust and simple process for separation of the biomolecules and their subsequent detection at very low concentrations. The use of magnetic nanoparticles to tag and separate biomolecules like nucleic acids is becoming very popular [22-24]. When the grain sizes of magnetic materials are changed to nanometre scale, the normal macroscopic domain structure transforms into a single domain state at a critical size. At this stage the magnetization reversal can happen from one magnetic easy axis to another via a magnetically hard direction[22, 25]. As a result of this rotation mechanism the magnetic nanoparticles have coercivities which are controllable and lies in the regime between soft materials and normal permanent magnetic materials. Magnetic nanoparticles used for bioseparation are generally Superparamagnetic, in which magnetization can randomly flip direction under the influence of temperature. These nanoparticles are composed of single domains and their diameters in the range of 3-50 nm. The nanoparticles lose their magnetization when the magnetic field is removed. This ability eliminates the use of centrifugation for separation as well as washing and is a simple process. Recently magnetic nanoparticles were used to selectively separate gram negative bacteria by tagging them with vancomycin[26, 27]. FePt nanoparticles were

functionalized with mercaptoalkanoic acid and used as an agent to bind histidine tagged proteins to separate them magnetically from the cell lysate[26-28]. Polymer and gold coated magnetite and haematite nanoparticles have been used to attach and separate antibodies[29, 30]. Polyethylenimine (PEI) have been used to purify plasmid DNA from bacterial cells and to develop a rapid protocol for extracting and purifying plasmid DNA from bacterial culture[31].

In chapter 1 we have synthesized gold coated magnetic nanoparticles and tagged it with capture probes consisting of oligonucleotides. It was used to separate and detect Raman label tagged oligonucleotides with specific sequences by SERS.

1.4 Graphene: A versatile material

Graphene is a single atomic plane of graphite where the carbon atoms are tightly packed in a two dimensional honeycomb lattice [32] as shown in Figure 1.4.

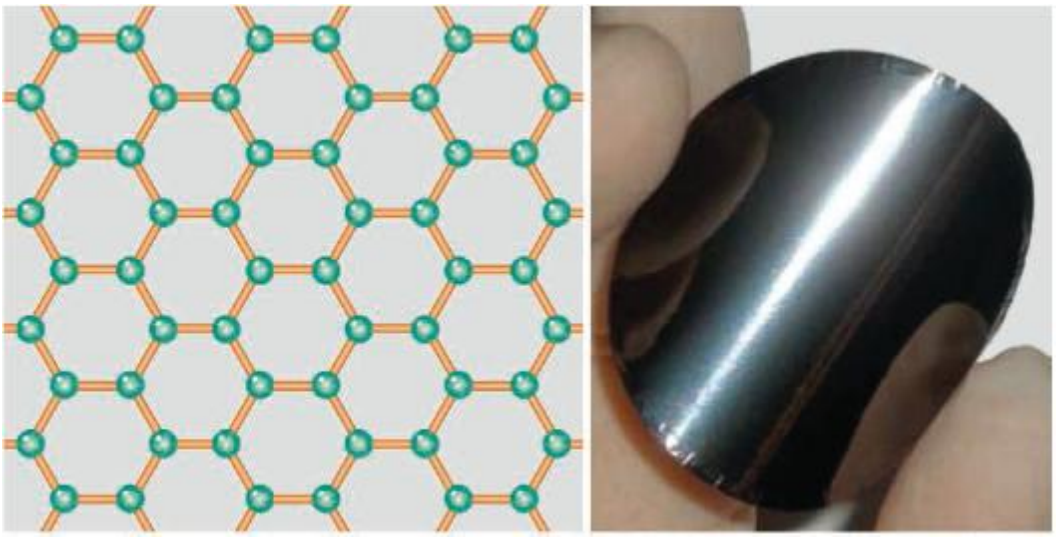

Figure 1.4 Carbon atoms (green dots) are bonded togetherthrough sp^2 hybridization. (Right) shiny and flexible graphene paper is formed bycontrolled restacking of graphene sheets[33]

Graphene displays unusual electrical properties arising from the confinement of electrons to two dimensions[32]. Apart from its unique electronic properties, graphene displays other unusual properties like good conduction of heat and electricity and it has a surface area more than double the finely divided activated carbon used for gas adsorption and water purification. These properties of graphene make them ideal candidates for nanoelectronics and nanoelectromechanical devices[32, 34]. The cost of synthesis of graphene is much less than carbon nanotubes and there are many ways to prepare graphene. Some of the methods are mechanical cleavage[32], epitaxial growth[35], bottom up organic synthesis[36], and chemical exfoliation[37]. Producing graphene in large amount is possible but to preserve its single layer characteristic is a challenge. In

this case the chemically derived graphene is the most stable in aqueous solutions. This is because of the chemical functionalization of the surface of the two dimensional flakes with oxygen containing groups which are hydrated in solution and also whose high negative charge stabilizes in solution and prevent them from agglomeration[38]. Successful dispersions and low cost of synthesis of graphene has made it technologically viable to make graphene based materials and devices. Graphene films can be made by drop casting, spraying, electrostatic adsorption, filtration, and dip or spin coating of graphene or precursor dispersions. Chemically functionalized graphene can be readily mixed with other polymer in solution producing a new class of electrically conductive nanocomposites which are less costly[39]. Easy synthesis of chemically derived graphene has helped it to be used in various nanoelectronic devices and also other areas too, like transparent electrodes for solar cells[40]. Graphene has the potential to be used in batteries and supercapacitors, separation technologies, catalysis support. Functionalization of graphene sheets can alter its conduction properties due to change in defect concentrations and also the adsorption characteristics.

In chapter 3 we have shown that adsorption of small molecules affects the D band of graphite oxide, which is a band formed due to the defects present. This property can be utilized for potential use in small molecule sensors.

1.5 Nanoarrays and multifunctional nanostructures

The fabrication of periodic nanoparticle array is of great interest as it opens up the possibility to be used in biosensors and chemical sensors because of their size dependent properties. These ordered patterns or arrays may also be used in optical and electronic devices and also as templates for growth of other nanostructures[41-44]. Typically the templates are generated with lithographic techniques such as colloidal lithography (CL) as shown in Figure 1.5, e-beam lithography and interferometric lithography and then the nanoparticles are selectively deposited into grooves or holes via suitable deposition methods such as dip or spin coating[45-47]. Few examples are illustrated in Figures 1.6 and 1.7. These self-assemblies mostly have a bottom up kind of oriented fabrication in which particles are added to the existing templates. Although many research works have demonstrated flexible, well defined patterns, it is still difficult to develop techniques in which the particles are patterned into small isolated areas and uniform over large areas.

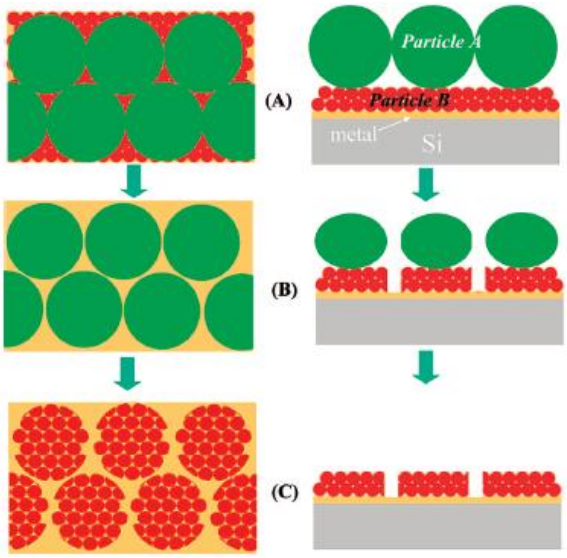

Figure 1.5 Schematic illustration of the fabrication of nanoparticles film patterns using colloidal lithography. Left column: top view; right column:side view. (A) A monolayer of self-assembled PS spheres atop a silica nanoparticle film and a thin metal film on a Si substrate. (B) After reactive ion etching of silica nanoparticle films with PS sphere mask. (C) After removal of etched PS spheres[48].

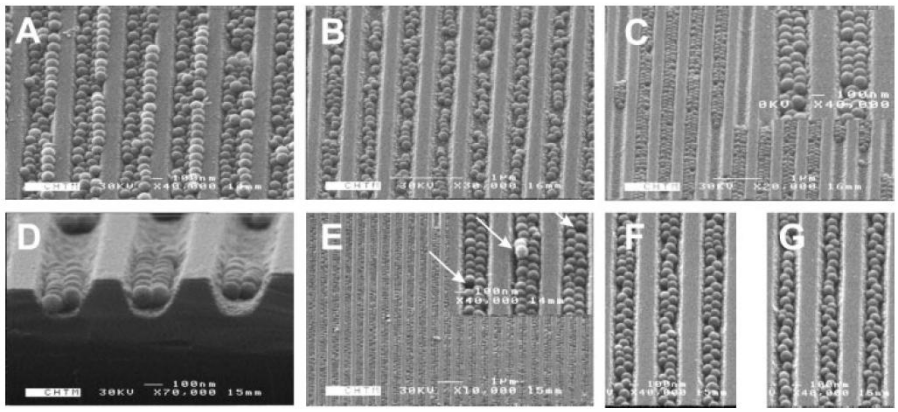

Figure 1.6 Field-emission scanning electron microscope (FESEM) images of ~80 nm diameter silica particles on grooved samples done by spin coating to self assemble the spheres[47].

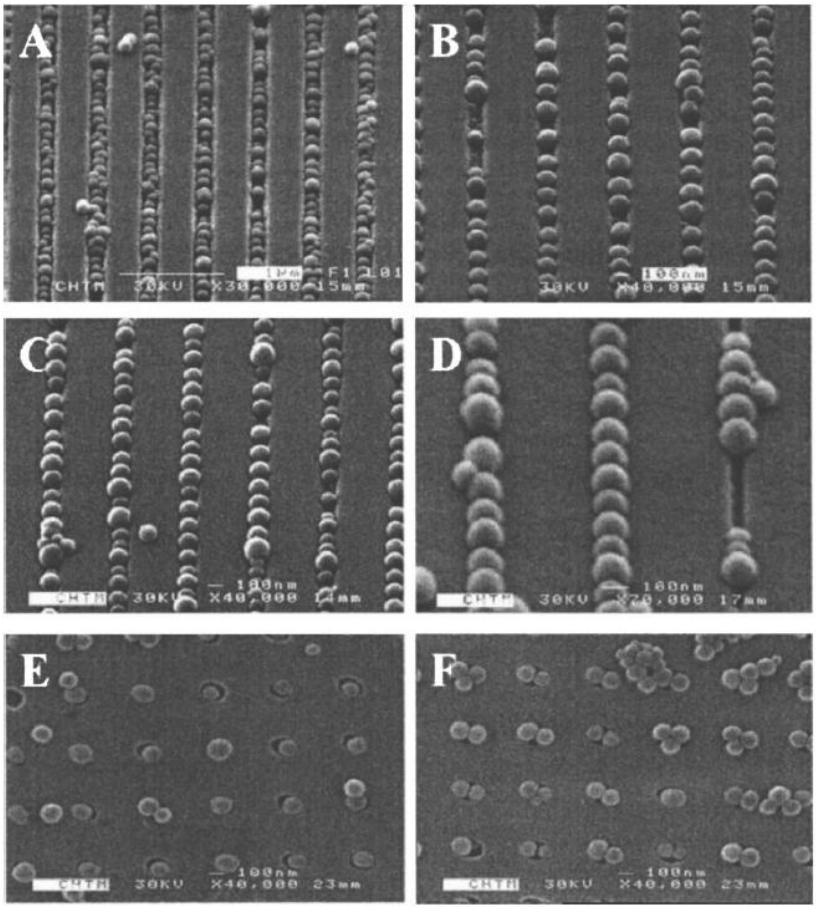

Figure 1.7 These pictures are examples of colloidal particles of silica under physical confinement[46].

Inorganic nanoparticles including noble metal, magnetic and semiconductor nanocrystal are emerging as a novel class of materials that have diverse applications like in medical applications, imaging and separation. Gold nanoparticles have been found to be useful in hyperthermal cancer treatment. Nanoparticles like quantum dots have been widely used as probes for optical imaging. Superparamagnetic nanoparticles have been widely used in bioseparation as well as targeted drug delivery applications. They have

also been used as MRI contrasting agents. These ordered structures, specially the nanostructures made up of noble metals like gold, silver and copper can be used for various applications. For SERS these kinds of arrays are necessary to give good enhancement factors. Gaining a control of the synthesis and ordering of the nanoparticles poses a challenge to create a substrate which can give reproducible SERS signal and also make it a quantitative tool.

1.6 References

[1] C. V. Raman and K.S. Krishnan, *Nature, 1928 , 121*, 501.

[2] F. Siebert, P. Hildebrandt, *Vibrational Spectroscopy in Life Science*, Wiley-VCH **2007**.

[3] B. Schrader, Infrared and Raman spectroscopy- Materials and Methods, VCH Publishers. Inc., New York, NY (USA) **1995**.

[4] D.A. Long, in , McGraw-Hill, London **1977**.

[5] M. Fleischman, P. J. Hendra, A. J. McQuillan, Chem. Phys. Lett. **1974**, 123.

[6] JeanmaireD.L., R. P. VanDuyne, J. Electroanal. Chem. **1977**, 1.

[7] M. G. Albrecht, J. A. Creighton, J. Am. Chem. Soc. **1977**, 5215.

[8] Surface Enhanced Raman Scattering- Physics and Applications, Springer-Verlag Berlin Heidelberg , **2006**, 1.

[9] S. Clancy, W. Brown, Translation: DNA to mRNA to protein, **2008**, 1.

[10] M. D. Bonnette, V. R. Pavlova, D. N. Rodier, L. P. Thompson, E. L. Boone, K. L. Brown, K. M. Meyer, M. B. Trevino, J. R. Champagne, T. D. Cruz, *Diagnostic Molecular Pathology* **2009**, *18*, 165.

[11] T. Demeke, G. R. Jenkins, *Analytical and Bioanalytical Chemistry* **2010**, *396*, 1977.

[12] A. Dorfman, N. Kumar, J. i. Hahm, *Langmuir* **2006**, *22*, 4890.

[13] P. Horakova-Brazdilova, M. Fojtova, K. Vytras, M. Fojta, *Sensors* **2008**, *8*, 193.

[14] R. McKendry, J. Y. Zhang, Y. Arntz, T. Strunz, M. Hegner, H. P. Lang, M. K. Baller, U. Certa, E. Meyer, H. J. Guntherodt, C. Gerber, *Proceedings of the National Academy of Sciences of the United States of America* **2002**, *99*, 9783.

[15] O. A. Sadik, A. O. Aluoch, A. L. Zhou, *Biosensors & Bioelectronics* **2009**, *24*, 2749.

[16] P. Aldeanueva-Potel, M. A. Correa-Duarte, R. ü. A. Alvarez-Puebla, L. M. Liz-Marzan, *ACS Applied Materials & Interfaces* **2010**, *2*, 19.

[17] R. A. Alvarez-Puebla, L. M. Liz-Marzan, *Small* **2010**, *6*, 604.

[18] S. Nie, S. R. Emory, *Science* **1997**, *275*, 1102.

[19] A. M. Polubotko, *Journal of Optics A-Pure and Applied Optics* **1999**, *1*, L18-L20.

[20] K. Kneipp, H. Kneipp, V. B. Kartha, R. Manoharan, G. Deinum, I. Itzkan, R. R. Dasari, M. S. Feld, *Phys. Rev. E* **1998**, *57*, R6281.

[21] Z. Y. Li, W. M. Tong, W. F. Stickle, D. L. Neiman, R. S. Williams, L. L. Hunter, A. A. Talin, D. Li, S. R. J. Brueck, *Langmuir* **2007**, *23*, 5135.

[22] S. Berensmeier, *Applied Microbiology and Biotechnology* **2006**, *73*, 495.

[23] A. Elaissari, *E-Polymers* **2005**.

[24] K. Obata, H. Tajima, M. Yohda, T. Matsunaga, *Pharmacogenomics* **2002**, *3*, 697.

[25] E. C. Stoner, *Philos. Trans. R. Sot. London* **1949**, *Ser. A52*, 562.

[26] H. W. Gu, P. L. Ho, K. W. T. Tsang, C. W. Yu, B. Xu, *Chemical Communications* **2003**, 1966.

[27] H. Gu, P. L. Ho, K. W. T. Tsang, L. Wang, B. Xu, *Journal of the American Chemical Society* **2003**, *125*, 15702.

[28] C. Xu, K. Xu, H. Gu, X. Zhong, Z. Guo, R. Zheng, X. Zhang, B. Xu, *Journal of the American Chemical Society* **2004**, *126*, 3392.

[29] G. K. Kouassi, J. Irudayaraj, *Analytical Chemistry* **2006**, *78*, 3234.

[30] S. L. Lu, J. Ramos, J. Forcada, *Macromolecular Symposia* **2009**, *281*, 89.

[31] C. L. Chiang, C. S. Sung, *Journal of Magnetism and Magnetic Materials* **2006**, *302*, 7.

[32] A. K. Geim, K. S. Novoselov, *Nat Mater* **2007**, *6*, 183.

[33] D. Li, M. B. Muller, S. Gilje, R. B. Kaner, G. G. Wallace, *Nat Nano* **2008**, *3*, 101.

[34] J. S. Bunch, A. M. van der Zande, S. S. Verbridge, I. W. Frank, D. M. Tanenbaum, J. M. Parpia, H. G. Craighead, P. L. McEuen, *Science* **2007**, *315*, 490.

[35] C. Berger, Z. Song, X. Li, X. Wu, N. Brown, C. Naud, D. Mayou, T. Li, J. Hass, A. N. Marchenkov, E. H. Conrad, P. N. First, W. A. de Heer, *Science* **2006**, *312*, 1191.

[36] J. Wu, W. Pisula, K. Mullen, *Chemical Reviews* **2007**, *107*, 718.

[37] G. Eda, G. Fanchini, M. Chhowalla, *Nat Nano* **2008**, *3*, 270.

[38] S. Stankovich, D. A. Dikin, R. D. Piner, K. A. Kohlhaas, A. Kleinhammes, Y. Jia, Y. Wu, S. T. Nguyen, R. S. Ruoff, *Carbon* **2007**, *45*, 1558.

[39] S. Stankovich, D. A. Dikin, G. H. B. Dommett, K. M. Kohlhaas, E. J. Zimney, E. A. Stach, R. D. Piner, S. T. Nguyen, R. S. Ruoff, *Nature* **2006**, *442*, 282.

[40] C. Gumez-Navarro, R. T. Weitz, A. M. Bittner, M. Scolari, A. Mews, M. Burghard, K. Kern, *Nano Letters* **2007**, *7*, 3499.

[41] A. J. Haes, L. Chang, W. L. Klein, R. P. Van Duyne, *Journal of the American Chemical Society* **2005**, *127*, 2264.

[42] C. A. Mirkin, R. L. Letsinger, R. C. Mucic, J. J. Storhoff, *Nature* **1996**, *382*, 607.

[43] R. W. J. Scott, S. M. Yang, N. Coombs, G. A. Ozin, D. E. Williams, *Advanced Functional Materials* **2003**, *13*, 225.

[44] J. M. Weissman, H. B. Sunkara, A. S. Tse, S. A. Asher, *Science* **1996**, *274*, 959.

[45] D. Y. Wang, H. Mohwald, *Advanced Materials* **2004**, *16*, 244.

[46] D. Y. Xia, S. R. J. Brueck, *Journal of Vacuum Science & Technology B* **2004**, *22*, 3415.

[47] D. Y. Xia, A. Biswas, D. Li, S. R. J. Brueck, *Advanced Materials* **2004**, *16*, 1427.

[48] D. Y. Xia, Z. Y. Ku, D. Li, S. R. J. Brueck, *Chemistry of Materials* **2008**, *20*, 1847.

Chapter 2

Nucleic acid capture and detection by SERS using oligonucleotide tagged magnetic core shell nanoparticles

2.1 Motivation

Most of the viral infections can be confirmed through immunoassays in which the patient's blood sample is screened by using specific viral antigens or antibodies specific to the viral antigen. Techniques like the immunofluorescence assays (IFA) or enzyme-linked immunosorbent assays (ELISA) are popularly used for clinical diagnosis[1]. But the major drawback of these techniques is that they fail to detect disease at the early stage due to low viral load or pre- seroconversion[2]. Long incubation times and cases of false positives are other drawbacks of these techniques. Conventional molecular techniques for viral nucleic acid detection are a tedious process comprising of numerous cycles of centrifugations for separations and washings. Also, techniques like PCR have been used extensively to detect nucleic acids from viruses and micro-organisms. PCR has high sensitivity but it has many drawbacks like it is expensive, and it requires a thermal cycler which is expensive and takes more than 12 hours for detection of nucleic acids[3]. Fluorescence assays which use PCR to amplify specific sequences of DNA and then detect them are real time detection techniques. But, the multiplexing capability of the real

time system is limited due to the emission profiles of the fluorophores, which can be broad and overlapping and also the sensitivity is dependent on efficient PCR cycling of the target sample[4].

SERS is an extremely sensitive technique and is capable of even single molecule detection[5, 6]. For getting optimal SERS signal there need to be some surface attachment properties added to nucleic acids to allow it to absorb into a metal surface and also a chromophore which will give a resonance contribution with the exciting laser wavelength, which will give a large increase in sensitivity. In order to do this a visible chromophore is attached to the probe. Different implementation schemes of SERS labels for DNA probing have been reported. Graham et. al. reported a method for detecting DNA on the adsorption of fluorophore labelled DNA onto colloidal silver particles which was subsequently detected by their respective SERS fingerprints[7]. Using the same scheme, eight commercially available fluorophores (ROX, rhodamine 6G, HEX, FAM, TET, Cy3, Cy5, TAMRA) were attached to the oligonucleotide strands[8]. Cao et. al. reported gold nanoparticle probes functionalized with oligonucleotides which were labelled with Raman-active dyes[9]. Wabuyele and Vo-Dingh developed a plasmonic nanoprobe composed of metal nanoparticles functionalized with a stem-loop DNA molecule tagged with Raman-active dyes. In the absence of the target DNA, the stem loop configuration of the probing single stranded DNA (ssDNA) kept the Raman label in close proximity to the metal nanoparticle to produce intense SERS signals. Upon hybridization with the target ssDNA, the stem-loop configuration of the probing ssDNA

was disrupted, and the Raman labels were physically separated from the metal nanoparticle, resulted in a quenching of the SERS signal[10]. SERS labeled DNA probes have been applied in bio diagnostics such as HIV detection[10], BRCA1 breast cancer gene detection[11], and in microfluidics[12]. Multiplex DNA detection using SERS labels have also been explored by Graham *et al.* to genotype the mutational status of the cystic fibrosis gene, regardless of whether it is a homozygote or heterozygote[7]. Six dissimilar DNA targets as well as two RNA targets with single nucleotide polymorphism were distinguished using six Ramanlabeled (Cy3, TAMRA, Texas-Red, Cy3.5, Rodamine 6G, Cy5) nanoparticles by Cao et al. Through careful design of probes and a consideration of surface adsorption, sensitive and specific DNA detection can be achieved[4].

In this chapter we present a technique which can be used as a simple to detect required sequences of nucleic acids by using Surface Enhanced Raman Spectroscopy (SERS). Few of the advantages of this method are fast and easy detection, simpler washing cycles and high sensitivity of detection. The schematic representations of this method are shown in Figures 2.1 and 2.2.

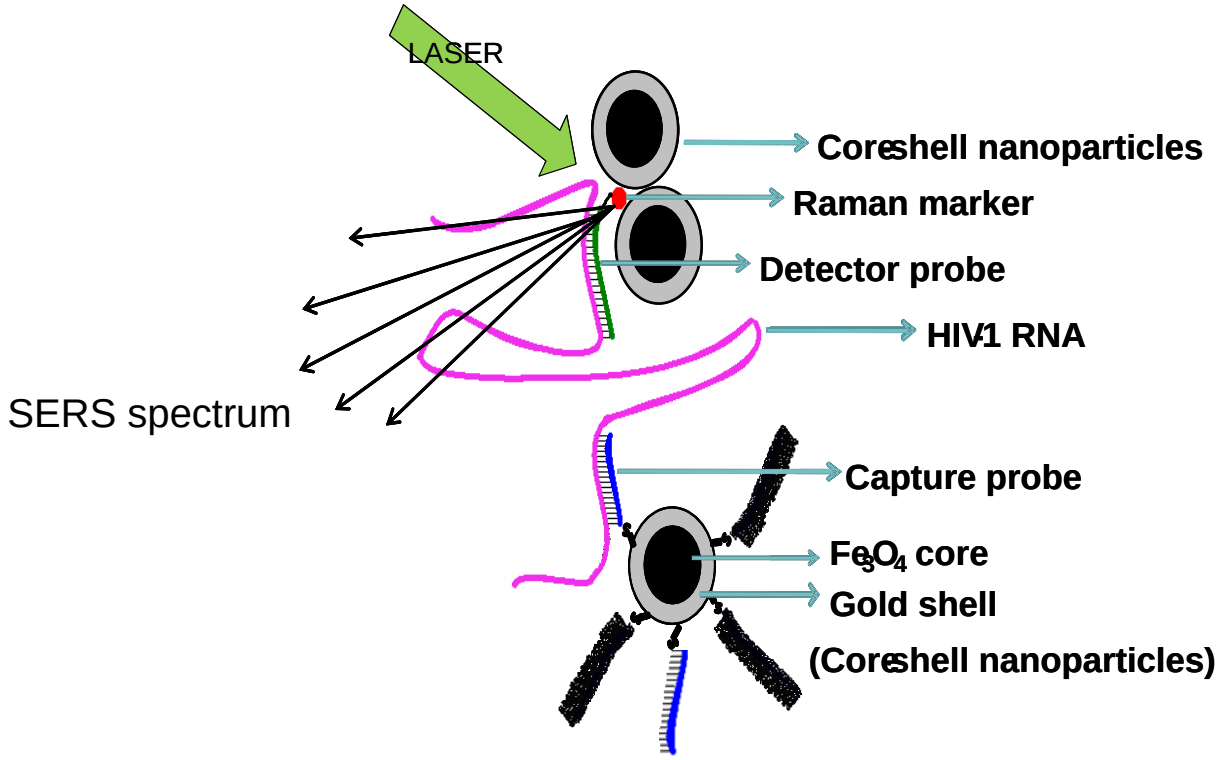

Figure 2.1 The schematic representation of capture of Nucleic acid and detection using SERS. A capture probe is tagged to the iron oxide core gold shell nanoparticle which captures the nucleic acid of specific sequence which is then tagged with detector probe . This detector probe contains a Raman marker which is detected by SERS.

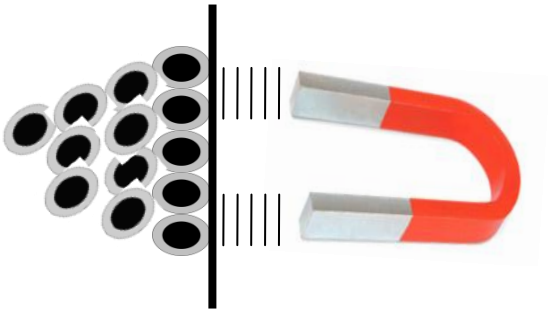

Figure 2.2 The superparamagnetic core shell nanoparticles can be easily separated by applying a magnetic field

2.2 Materials and methods

2.2.1 Preparation of gold coated iron oxide nanoparticles

The synthesis of gold nanoparticles was done by a modified procedure proposed by Lin et al.[13] by a reverse micellar method. Cetyltrimethylammonium bromide (CTAB) reverse micelles with 1-butanol as co-surfactant and iso-octane as oil phase were used to first produce iron oxide nanoparticles and subsequently aurochloric acid was reduced on to the surface of these iron oxide nanoparticles. The size of the reverse micelle is dependent on the molar ration of water to surfactant.

A solution labelled A was prepared with $FeCl_3.6H_2O$ (0.129 g), $FeCl_2.4H_20$ (0.0472 g), 0.6001 g of CTAB, 0.5 g of butanol (0.6174 mL) and 5 g of iso-octane (2.190 mL). 0.4740 mL of water was also added to maintain the molar ration of water to CTAB

at 8. Solution B was prepared using 0.1021 g of $NaBH_4$ and 0.6 g of CTAB in solution with 0.5 g of butanol (0.6174 mL) and 5 g iso-octane (2.190 mL).2.5 mL of solutions A and B were mixed for 35 minutes in a beaker with non-magnetic stirring at 60 ^oC.

Fe_3O_4 nanoparticles were thus prepared (I). Solution C was prepared by mixing 0.06456g of aurochloric acid with 0.3 g of CTAB, 0.3087 mL of butanol, 1.4534 mL of iso-octane and 0.1066 g of $NaBH_4$. 2 mL of each solutions of C and D are added to solution (I) with the addition of 0.5 M NaOH at different intervals such that the pH was maintained between 10 and 12. The solution was mixed with a non-magnetic stirrer for 15 minutes. The resultant nanoparticles were washed four times with water and four times with methanol. The nanoparticles were re dispersed in the same amount of water as the reactant volume.

2.2.2 Constitution of thiol modified oligonucleotides

5' end thiol modified oligonucleotides were bought from Bioserve india. The sequence of oligo used as capture probe was 5' HS-CCG TCT GTT GTG TGA CTC TGG TAACT 3' and the detector probe was 5’ R6G-AGTTA CCA GAG TCA CAC AAC AGA CGG 3’. The thiol modified oligo was dissolved in tris-EDTA (TE) buffer to a final concentration of 1μg/μL.

2.2.3 DTT treatment and purification of stored thiol modified oligo

When the solution of thiol modified oligo is stored in solution there is a possibility that the thiol group gets oxidized to form a dimer consisting a disulphide bond. In order to cleave this bond to get back the thiol group, Dithiothreitol (DTT) is used. 200 mL of 1X PBS was taken to make a solution of 0.1M DTT. 2 mg of thiol modified oligo was added to this solution. The components were mixed and incubated at room temperature for 1 hour. Purification was done in a G-50 matrix. G-50 matrix was reconstituted in PBS and packed into a column of 1mL syringe. The total volume is 1 mL. The column was spun at 5000 rpm for 1 min to remove PBS. DTT treated oligo was added to this column and spun at 5000 rpm for 1 min. The flow through was collected to get the purified thiol modified oligo. The purified oligo was used immediately for binding.

2.2.4 Binding of oligo to core shell nanoparticles

200 μL of nanoparticles solution and 1 μL of capture probe solution was mixed together and sonicated for 1 min. The solution was incubated at room temperature for 24 hours.

2.2.5 Hybridization of capture probe with detector probe

The capture probe attached nanoparticles were washed several times with millipore water by magnetic separation. The nanoparticles were magnetically separated and reconstituted in 50 μL of 1X PBS buffer. 1 μL of detector probe solution was added to it. It was incubated for 15 minutes at 65^{o}C and for 1 hr at 37^{o}C. After hybridization the solution was washed with 1X PBS solution.

2.2.6 Preparation of samples for SERS

After giving the hybridized sample several washes, equal volume of the core shell nanoparticle solution was added to the sample. The sample was drop cast onto a glass substrate and dried. SERS spectra were taken using a 632 nm He-Ne laser. The slit width was 0.2 μm and grating used was 1800 cm^{-1}. Accumulation time was 60 seconds.

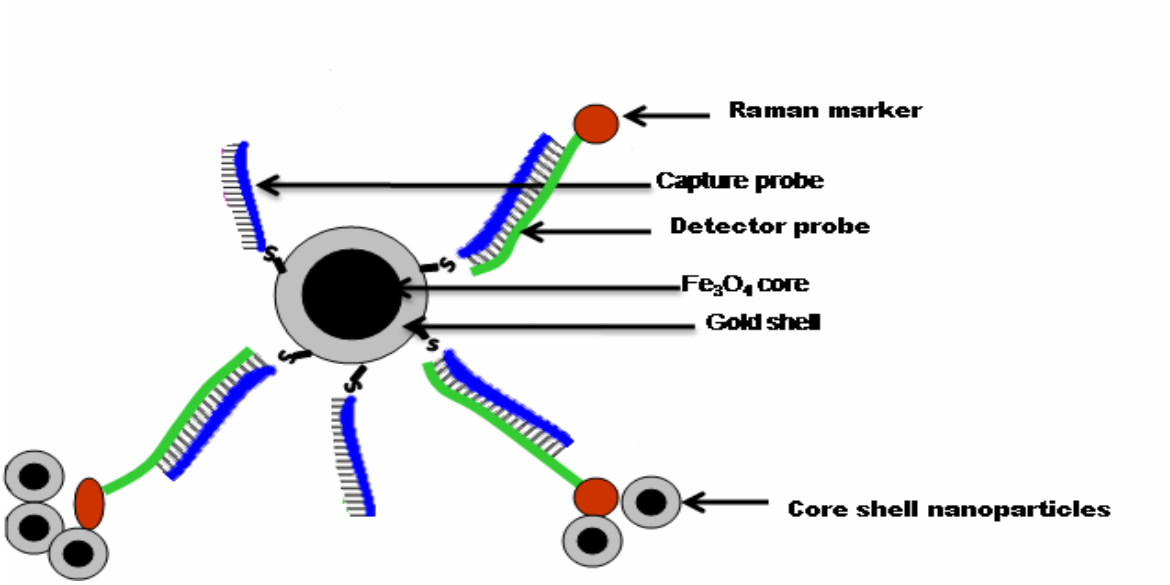

Figure 2.3 Proof of: For showing that oligonucleotides can be captured and detected by concept using magnetic core shell nanoparticles, a detector probe was directly captured and its presence was proved by SERS

2.3 Results and discussions

2.3.1 Characterization of core shell iron oxide nanoparticles

The gold coated iron oxides were found to be 10-12 nm in diameter and showed super-paramagnetic behavior which is shown in the Figure 1.4. The EDAX spectrum

(Figure 1.5) shows the presence of gold on the surface of these nanoparticles. The magnetic measurement of the core shell nanoparticles shows that these are superparamagnetic in nature. The hysteresis loop shows that both the magnetic remnance and coercivity is zero. This is a useful property of the nanoparticle for separation and washing. After separation the magnetic nanoparticles can easily be redispersed into aqueous medium without any aggregation due to remnant magnetic field. Also the superparamagnetic nanoparticles have magnetic susceptibility more than the paramagnetic materials. This makes the nanoparticles strongly attracted to magnet thereby saving time in washing cycles. Figure 1.3 shows the schematic diagram of the process.

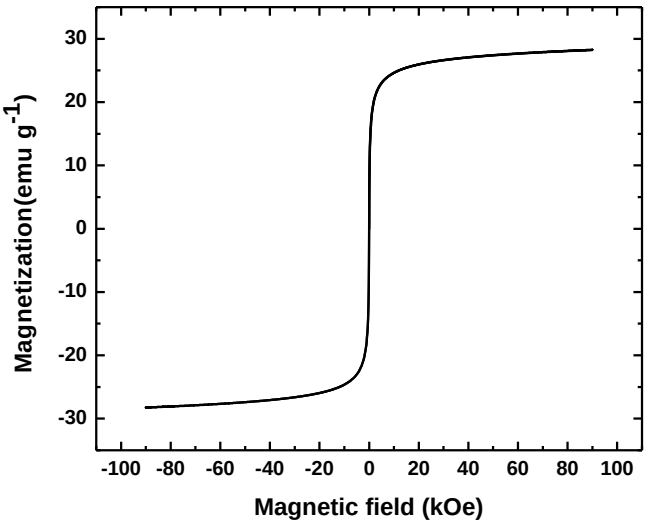

Figure 2.4 Magnetic hysteresis curve of magnetite core gold shell nanoparticles. The hysteresis shows superparamagnetic behaviour of the nanoparticles.

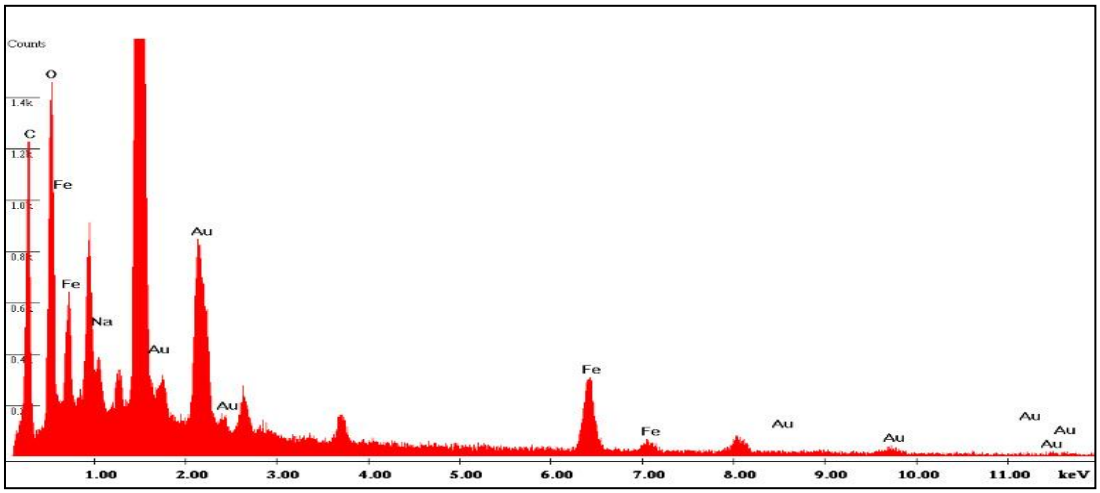

Figure 2.5 The EDAX spectrum of the magnetite core gold shell nanoparticles.

2.3.2 Attachment of oligonucleotide to core shell nanoparticles

The capture probes were attached to the gold coated surface of the magnetite nanoparticles. The gold thiol binding is very well known and forms a strong bond a pictorial representation of which is shown in Figure 2.6.

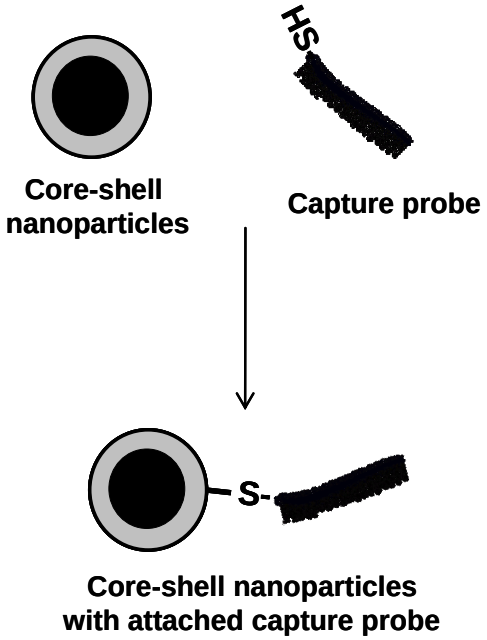

Figure 2.6 A pictorial representation of the gold thiol chemistry used to attach the thiolated capture probe to the core shell nanoparticles

ince the oligonucleotides have a very high negative charge, after capping of the coreshell nanoparticles they become highly negatively charged and the negative charge increases with the loading of oligonucleotides. The zeta potentials of the core shell nanoparticles before and after capping with capture probe is shown in Figures 2.8 and 2.9 and the variation of zeta potential of with loading of capture probe is shown if Figure 2.10. From the UV-vis spectra (Figure 2.7), we can see that before attachment of the capture probe the nanoparticles are somewhat aggregated which is evident from the broadness of the

peak. After the attachment of the capture probe the peak becomes sharper as the nanoparticles are now capped with a highly negatively charged molecule which repels each other.

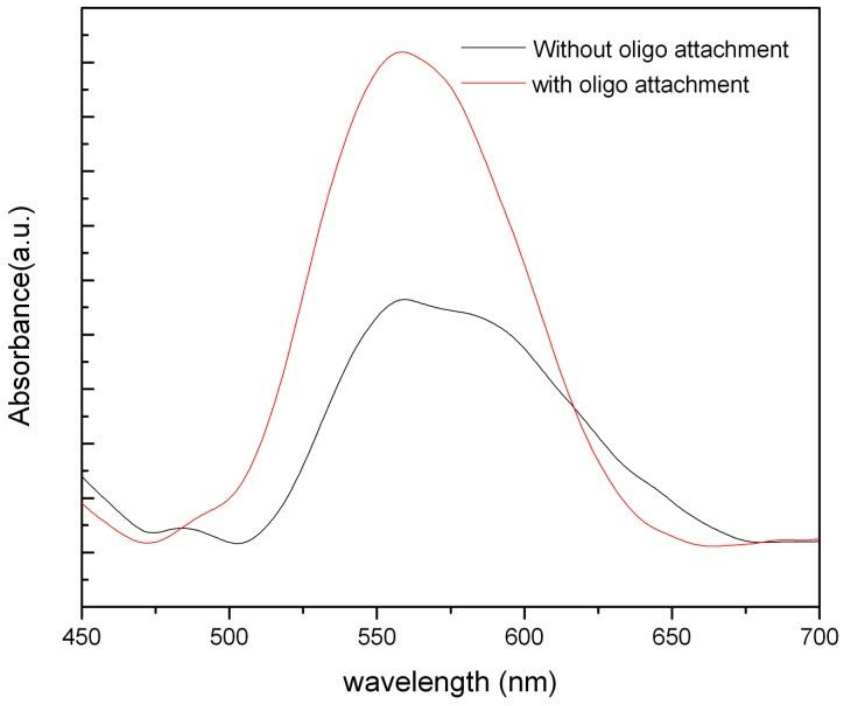

Figure 2.7 The UV- vis spectra of the core shell nanoparticles before and after the attachment of the capture probe.

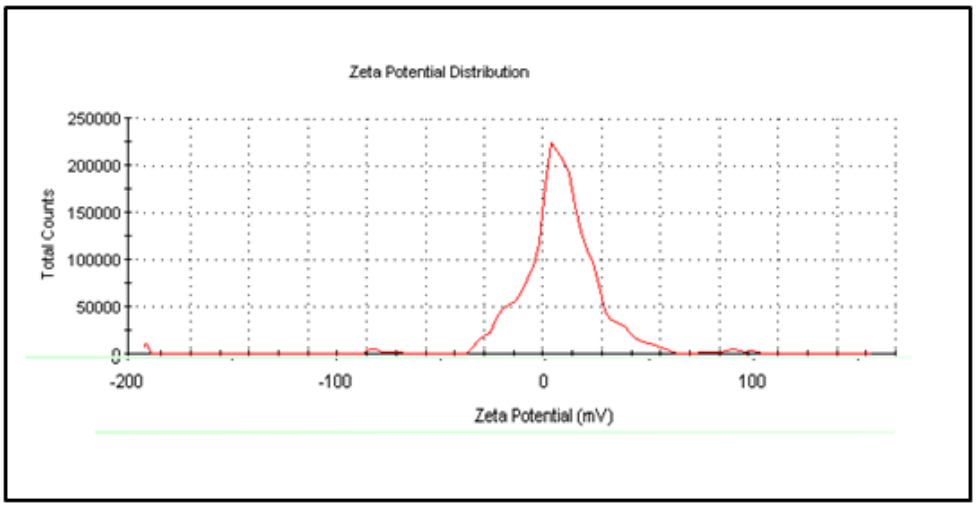

Figure 2.8 The zeta potential of the core shell nanoparticles before attachment of capture probes

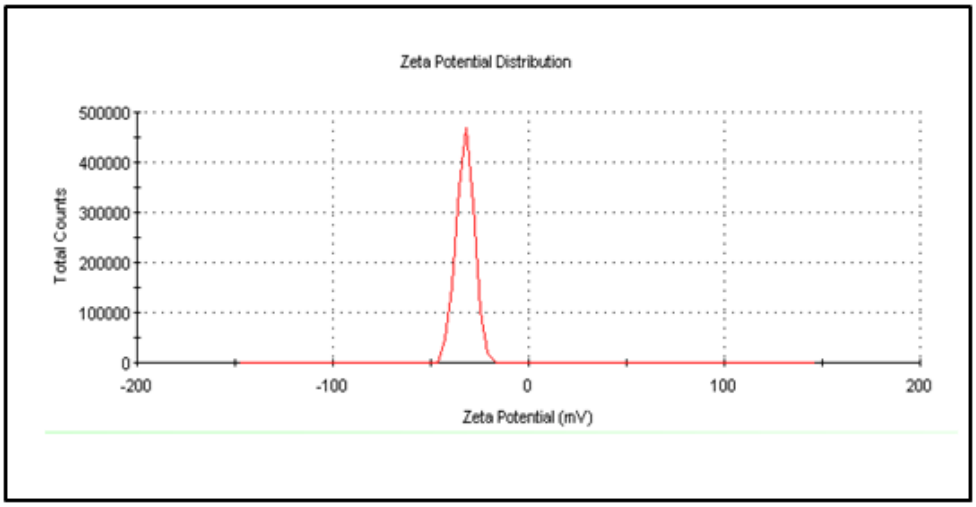

Figure 2.9 Zeta potential of core shell nanoparticles after attachment of capture probe

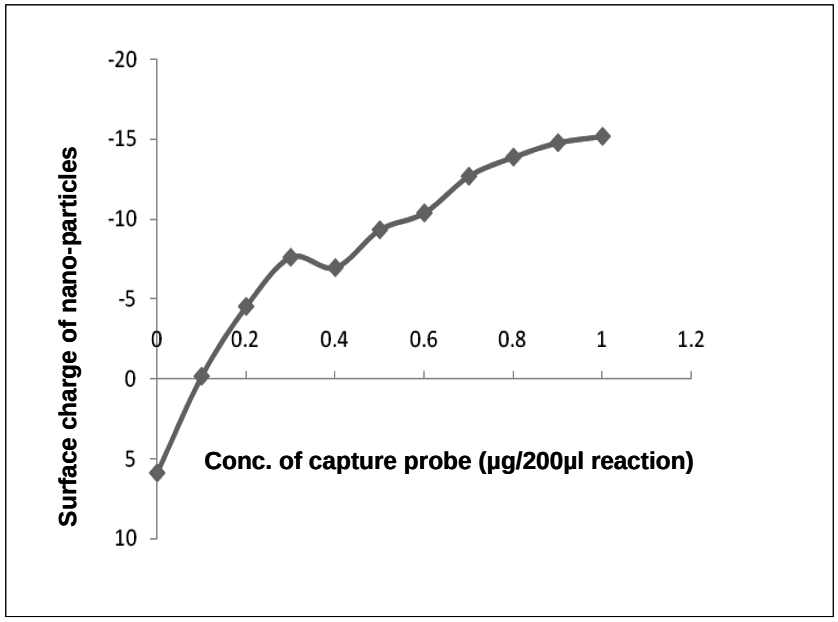

Figure 2.10 The variation of zeta potential of the core shell nanoparticles with different loading of capture probe.

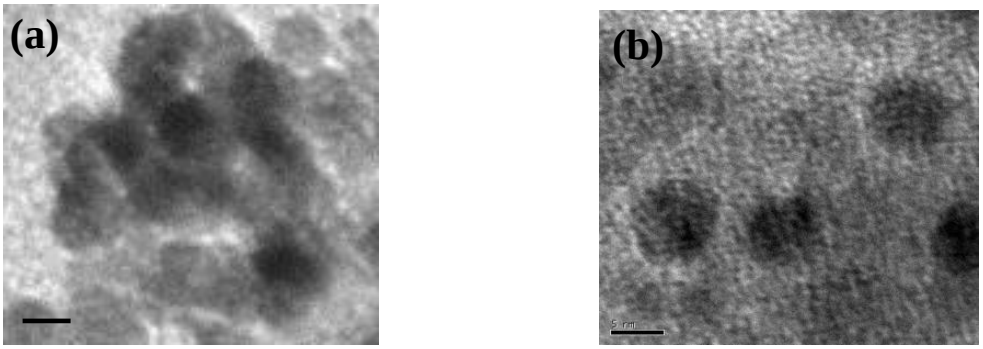

Figure 2.11 (a) TEM image of the core shell nanoparticles before tagging with capture probe, and (b) after tagging with capture probe. The scale bars of both the images are 5 nm.

2.3.3 Hybridization of capture probe tagged core shell nanoparticles with detectore probe.

The capture probe tagged core shell nanoparticles were put in hybridizing conditions with detector probe. Two types of detector probes were used. One of them had complementary base sequences with the capture probe and the other had non complementary base sequences with the capture probe. This was to test whether the detector probe binds to the nanoparticles non-specifically. It is essential to test the non specific adsorbtion of the detector probe because presence of non specific attachment can give rise to false positive results. From these experiments we observe that after hybridization and after several cycles of washing magnetically we get good SERS signal of R6G which is attached to the detector probe. This is quite advantageous as there is no need to add different kinds of nanoparticles to the system for enhancing the signals of R6G. The same gold coated magnetite coreshell nanoparticles are suitable for getting good SERS signal. We also observe that after hybridization and washing cycles the addition of some extra volume of the stock core shell nanoparticles gives better SERS signals (Figure 2.13). While there is no spectra from washed nanoparticles alone (Figure 2.12). This can be due to the fact that since the core-shell nanoparticles are already tagged with capture probe and are highly negatively charged, the R6G molecule is not able to come to close proximity of the nanoparticles to give good enhancement. But on addition of fresh nanoparticles with almost no negative charge allows the R6G dye molecules to easily bind to these nanoparticles thus giving good SERS enhancements.

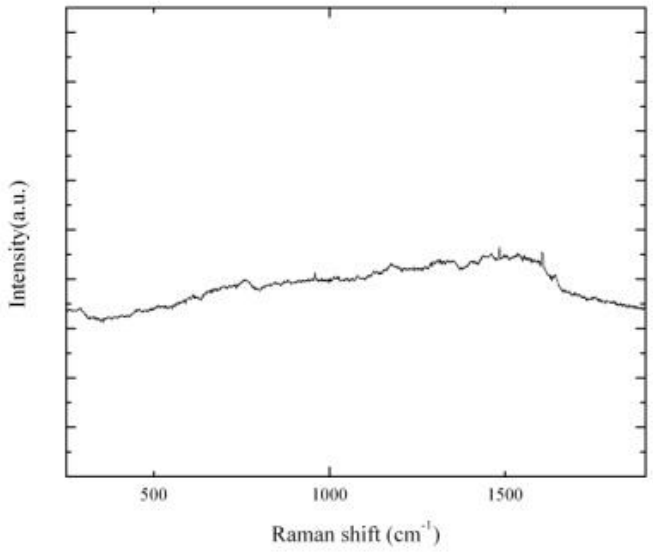

Figure 2.12 Raman spectra of capture probe tagged coreshell nanoparticles. It shows no observable peaks.

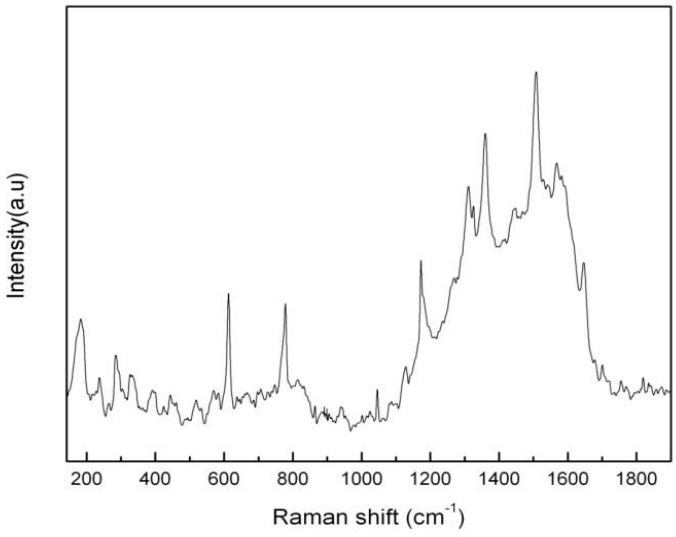

Figure 2.13 SERS spectra obtained after hybridization between capture and detector probes shows the characteristics of R6G

For the hybridization experiment where non complementary base sequences were used of capture and detector probe, after several washing cycles we didn't get any observable SERS signal from the nanoparticles which indicates that the hybridization didn't happen as expected (Figure 2.14). Also there was an absence of non specific adsorbtion which is also expected as the capture probe makes the core shell nanoparticles negatively charged. Any approaching detector probe which is also negatively charged cannot adsorb non-specifically without having any kind hybridization with the capture probe. On the other hand we see that the supernatant after the first wash gives good SERS spectra of R6G on addition of core shell nanoparticles (Figure 2.15). This shows that the R6G attached detector probe was present in the system but didn't get attached to the capture probe.

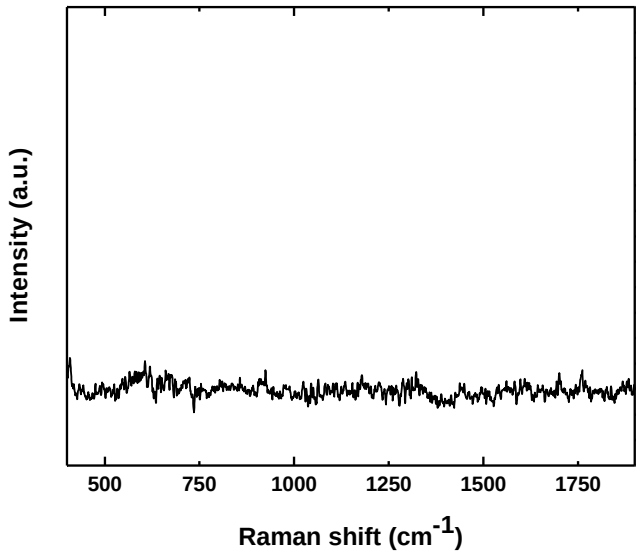

Figure 2.14 Raman spectra obtained in the experiment where non complementary base sequences of capture and detector probes were used.

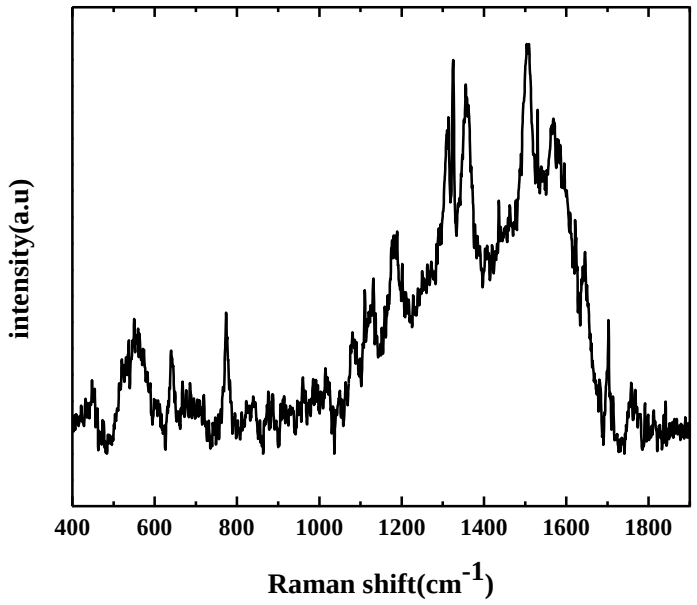

Figure 2.15 The supernatant after the first wash gives SERS spectra of R6G

From these experiments it is shown that oligonucleotides of specific base sequences can be captured using oligonucleotide capped core shell magnetic nanoparticles. This technique has an advantage over other techniques which uses a solid support for immobilization and hybridization of nucleic acids or antibodies for biological assays. This is because the hybridization occurs in a mobile phase over the surface of nanoparticles. The hybridization efficiency is much more in this case. Therefore detection of ultra low concentration of analytes will be possible. Also the development of SERS techniques as well as the capability of detecting even single molecules using SERS will also help in pushing this limit of detection to much lower limits.

2.4 Conclusion and future scope of work

In this work we have shown that core shell superparamagnetic nanoparticles can be used in separation and detection of nucleic acid sequences by the use of SERS. Work on showing the detection of actual viral RNA is being undertaken and also the limit of detection of these nucleic acids. This technique is technologically important due to the ease of preparation of the samples, easier washing cycles and high sensitivity of detection. This technique is also a low cost one as it involves low cost diode lasers. This method is technically less challenging and also cost and time efficient. This technique also has the potential to diagnose a wide variety of diseases like HIV, dengue, malaria, polio, tuberculosis etc. and there is a possibility for multiplexing too. Therefore this technique can have a broader application with minimum resources.

2.5 References

[1] L. Yobas, W. Hui, H. M. Ji, Y. Chen, S. S. I. Liw, J. Li, C. S. Chong, X. Ling, C. K. Heng, H. J. Lye, S. R. Bte, K. Lee, S. Swarup, S. M. Wong, T. M. Lim, *2005 IEEE Sensors, Vols 1 and 2* **2005**, 49.

[2] S. X. Tang, I. Hewlett, *Journal of Infectious Diseases* **2010**, *201*, S59-S64.

[3] W. Usawattanakul, A. Jittmittraphap, P. Tapchaisri, K. Siripanichgon, K. Buchachart, A. Hong-ngarm, P. Thongtaradol, T. P. Endy, *Dengue bulletin* **2002**, *26*, 131.

[4] D. Graham, K. Faulds, *Chemical Society Reviews* **2008**, *37*, 1042.

[5] S. Nie, S. R. Emory, *Science* **1997**, *275*, 1102.

[6] A. M. Polubotko, *Journal of Optics A-Pure and Applied Optics* **1999**, *1*, L18-L20.

[7] D. Graham, W. E. Smith, A. M. T. Linacre, C. H. Munro, N. D. Watson, P. C. White, *Analytical Chemistry* **1997**, *69*, 4703.

[8] K. Faulds, W. E. Smith, D. Graham, *Analytical Chemistry* **2003**, *76*, 412.

[9] Y. C. Cao, R. Jin, C. A. Mirkin, *Science* **2002**, *297*, 1536.

[10] M. B. Wabuyele, T. Vo-Dinh, *Analytical Chemistry* **2005**, *77*, 7810.

[11] M. Culha, D. Stokes, L. R. Allain, T. Vo-Dinh, *Analytical Chemistry* **2003**, *75*, 6196.

[12] T. Park, S. Lee, G. H. Seong, J. Choo, E. K. Lee, Y. S. Kim, W. H. Ji, S. Y. Hwang, D. G. Gweon, S. Lee, *Lab on A Chip* **2005**, *5*, 437.

[13] J. Lin, W. Zhou, A. Kumbhar, J. Wiemann, J. Fang, E. E. Carpenter, C. J. O'Connor, *Journal of Solid State Chemistry* **2001**, *159*, 26.

Chapter 3

Molecule sensing with graphite oxide

3.1 Motivation

Molecular detection using nanomaterials is a promising area of nanotechnology. Graphene as well as Graphite oxide have become potential candidates for making molecular sensors because of the fact that all the atoms are located on the surface and the therefore various properties of these materials changes on the adsorption of molecules. The same is true for another kind of carbon based nanomaterials called carbon nanotubes. Single walled carbon nanotubes have been used to make for detection of gases and chemicals[1, 2]. There are reports of single walled carbon nanotubes which were used for sensing NH_3 and NO_2[3, 4]. These molecules interact with the nanotubes and a charge transduction takes place and the adsorbed molecules can be detected by monitoring the change in electrical resistance. Several molecules like acetone and ammonia interact weakly with the nanotubes with different energies, charge transfer and polarizability. It has been shown that the adsorpt ion and desorption energies of the molecules are influenced by the defect sites of these carbon nanotubes[5]. These nanotube defects form low-energy sorption sites which serve as nucleation sites for additional condensation of

A manuscript is under preparation based on the work done in this chapter.

analyte vapor. These defects were mainly created by carboxylic acid groups which were introduced along the walls of the carbon nanotube (Figure 3.1a).

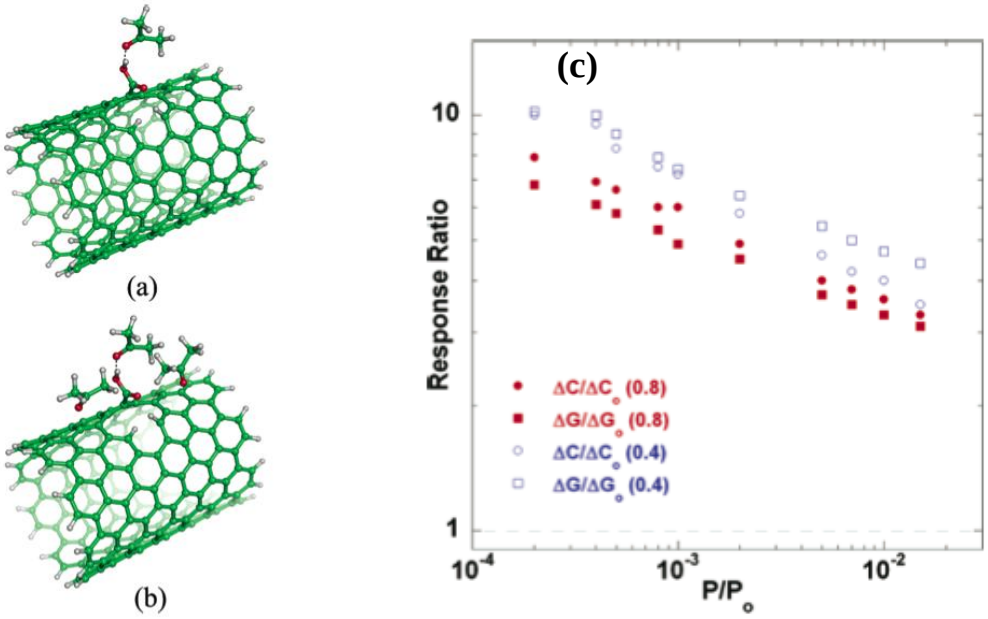

Figure 3.1 Binding of a carboxylic acid defect on a Single walled carbon nanotube. (b) Clustering of acetone around the defect via intermolecular bonding. (c) Response ratio of carbon nanotube network sensors to acetone following oxidation[5].

Graphene can be considered very close to carbon nanotube as the latter can be considered as a rolled up graphene. Normally just like carbon nanotube the change in electron transport of graphene is employed to sense adsorbed molecules on the surface. Reduced graphene oxide is shown to be used as a gas and molecule sensor [3, 6-8]. Graphene oxide is easily produced in large amounts by chemical exfoliation of graphite

and dispersing it in aqueous medium. It can be called as chemically modified graphene and it contains oxygen functional groups like epoxides, alcohols and carboxylic acids. The carbon to oxygen ration is shown to be three to one[8]. These oxygen containing groups constitute energetic sites for chemical adsorption, especially for polar molecules.

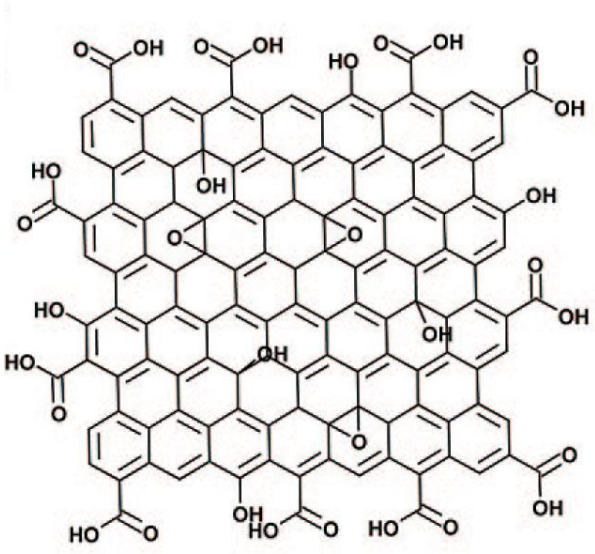

Figure 3.2 Structure of Graphite oxide with carboxyl, epoxy and hydroxyl groups.

In this work we show how the defect band of graphite oxide shifts in response to the adsorption of small molecules like glucose and amino acids. These biologically relevant molecules contain oxygen containing polar groups (Figure 3.2) and get adsorbed to the hydrophilic defects sites on the graphite oxide. These D band shifts in the Raman

spectra have the potential to be used as a detection tool for molecules like glucose which is easy to prepare and takes less time.

3.2 Materials and methods

3.2.1 Preparation of graphite oxide

The exfoliation and oxidation of graphite flakes were done according to methods reported in literature[9].The exfoliation of natural graphite particles (particle size 300-400 μm, Sratmin Graphite, NJ) was carried out as follows. Natural graphite particles were intercalated by immersing the particles in a mixture of conc. H_2SO_4/HNO_3 (3:1 by volume) for 24 hrs at ambient conditions. The material was washed with distilled water and air-dried. Exfoliation was carried out by introducing the material in a preheated furnace at 800 ^oC for a minute in air. The puffed- up material is taken out of the furnace and stored in a desiccator for further use. EG was first subjected to ultrasonication in acetone for 1 h. The powdered EG was dried well and further oxidation was carried out by Hummers method by immersing the EG (200 mg) particles in conc H_2SO_4 (6 mL) and adding $KMnO_4$ (6 g) slowly in small quantities while the temperature was maintained between 0 and 5 ^oC using ice bath. After the complete addition of $KMnO_4$, the mixture was heated to 37 ^oC and kept at this temperature for 30 min. Distilled water (92 mL) was then slowly added. The temperature of the mixture was raised to 95 ^oC and maintained

for about 15 min. The mixture was further diluted with 280 mL of water and later 20 mL of 30% $H_2O_2$was added. The resulting solid was then filtered off and washed with 5% HCl until the filtrate was free from sulfate ions. The EGO thus obtained was further washed thoroughly with water and dried in air for 24 hrs and stored over phosphorus pentoxide. A colloidal suspension of EGO (1mg/mL) was prepared by dispersing it in water by ultrasonication. The samples were ultracentrifuges at 8000 rpm for 15 mins to remove the undissolved particles and spin coated for AFM imaging.

3.2.2 Preparation of samples for Raman

The reagents were obtained from Sigma Aldrich. Solutions of glucose, lysine and aspartic acid were prepared in water. 5 µl of this solution was mixed with same amount of the above prepared graphite oxide solution and was sonicated for 15 mins. 1 µl of this solution was drop coated on a silicon wafer for Raman measurements.

3.3 Results and discussions

The Graphite oxide (GO) produced by exfoliation and oxidation showed D band peak at ~1345 cm^{-1} and a G band peak at around 1600 cm^{-1}. The Raman spectrum of graphite has been reported to show bands at ~1370, ~1583, ~1620, ~2700, and ~3200 cm-1, designated as D, G, D′, G′, and D″ bands respectively. The G band shifts to a lower wavenumber in case of GO because of reduced number of sheets resulting in a blue shift[10], overlap of G band with D′ which becomes active because of the defects[11] and the presence of double bonds separated by functional groups on the carbon network of GO[12]. The shift of D band towards lower wave numbers is because of the introduction of more sp^3 character[12].

From Figure 3(b) we can see that with increasing concentration of glucose, the D band shows shift towards lower wave number while the position of G band remains the same. The increase in the D band shift (see Figure 3.3(ii)) is not linear but remains a saturation value after reaching a certain concentration. This is expected as more and more glucose molecules gets attached to the oxygen rich sites on the graphite oxide sheet and soon it reaches a point where the all the sites are already occupied by the glucose molecules. It is interesting to note that the saturation value is 1333 cm^{-1}, which is the characteristic mode of diamond. Incidentally, it signifies a large increase in sp^3 character, expected when the molecules attach to the oxygen rich sites on GO.

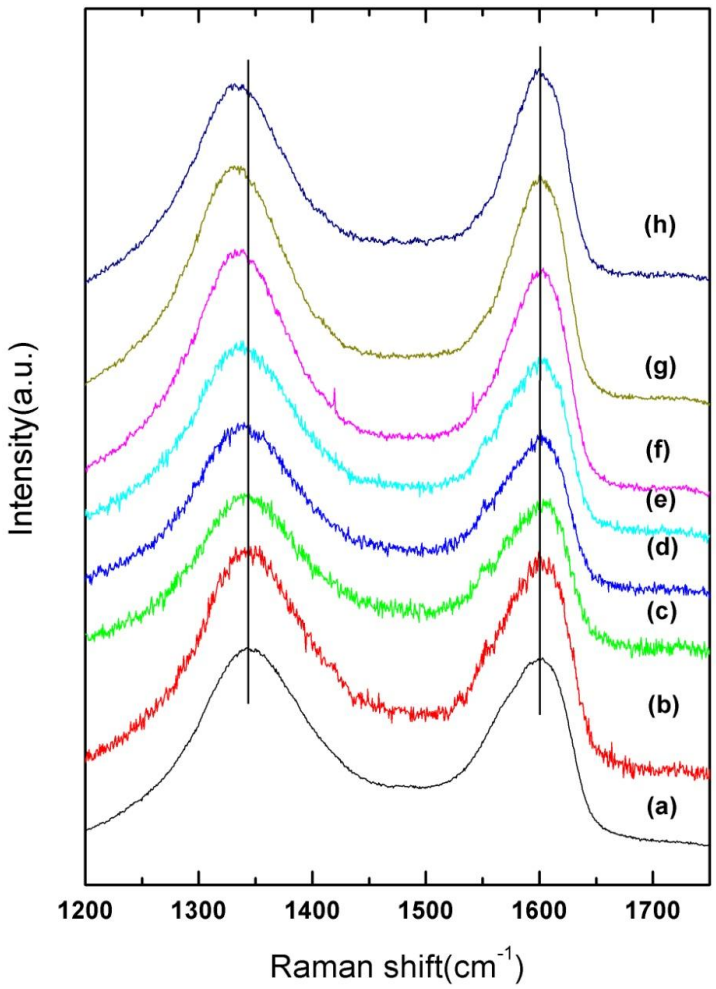

Figure 3.3(i) Raman spectra of Graphite oxide mixed with glucose with varying concentrations. In spectras a to h the concentration of glucose with fixed concentration of GO are 0.01 mM, 0.1 mM, 0.2 mM, 0.5 mM, 1 mM, 10 mM,100 mM respectively.

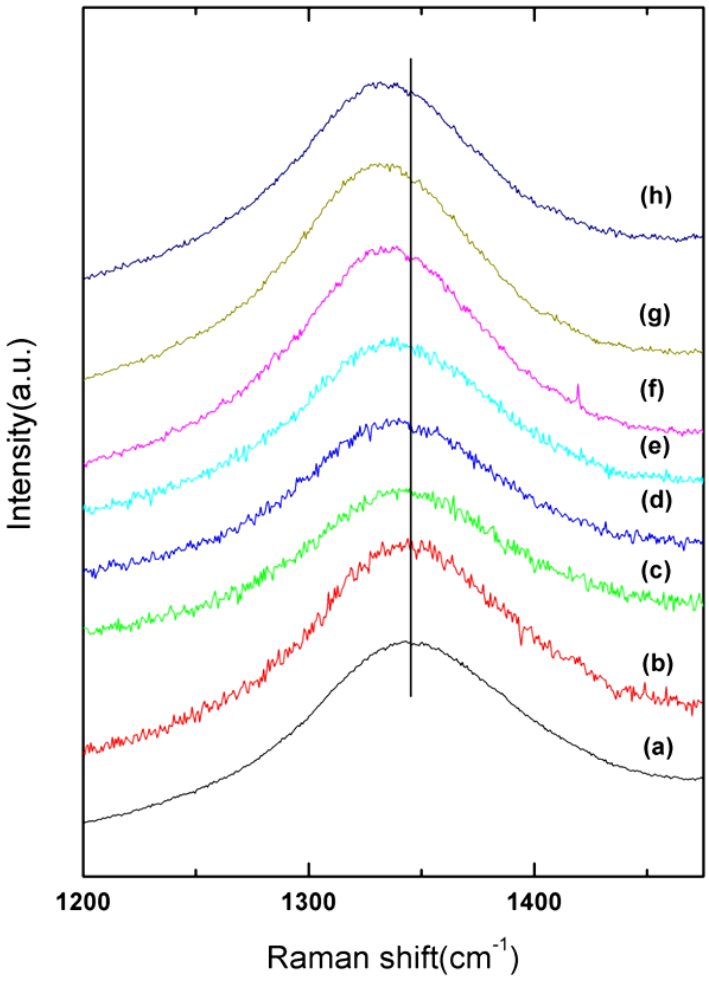

Figure 3.3(ii) The D bands of the samples. In spectras a to h the concentration of glucose with fixed concentration of GO are 0.01 mM, 0.1 mM, 0.2 mM, 0.5 mM, 1 mM, 10 mM,100 mM respectively.

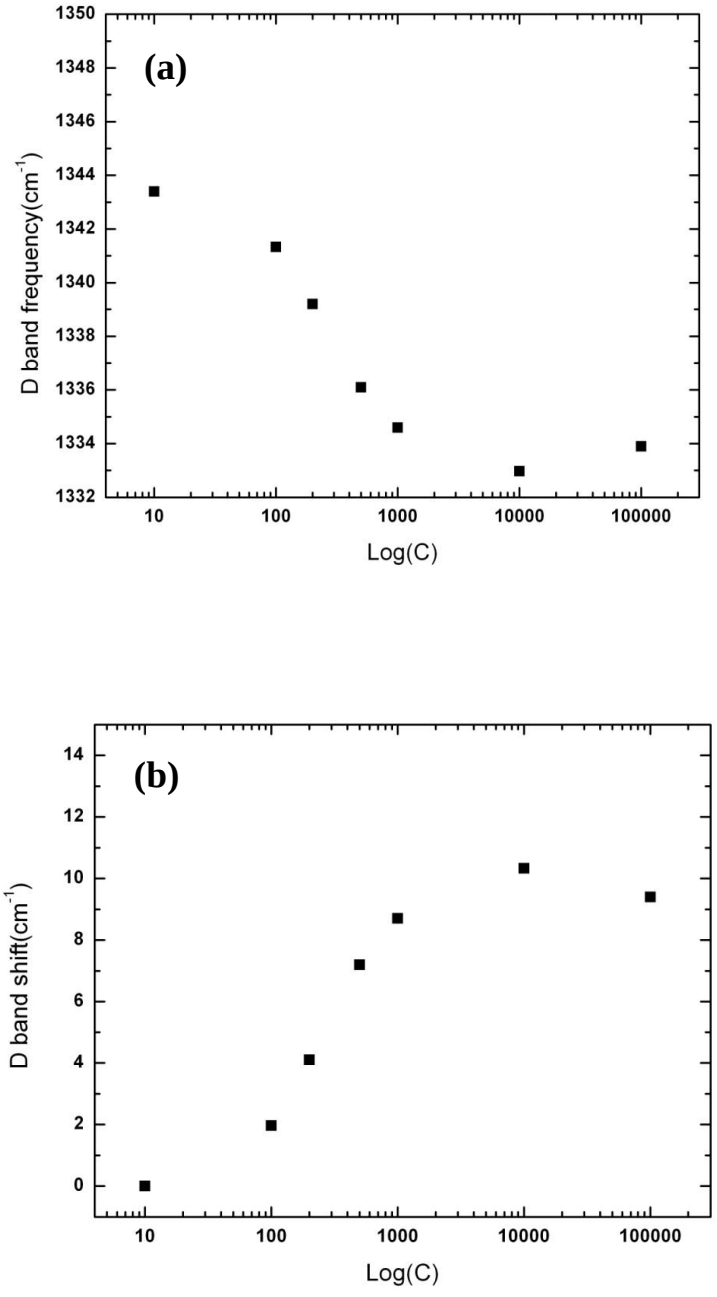

Figure 3.3(iii)(a) D band frequencies and (b) D band shifts, at different concentrations of glucose. Concentration C is in µM.

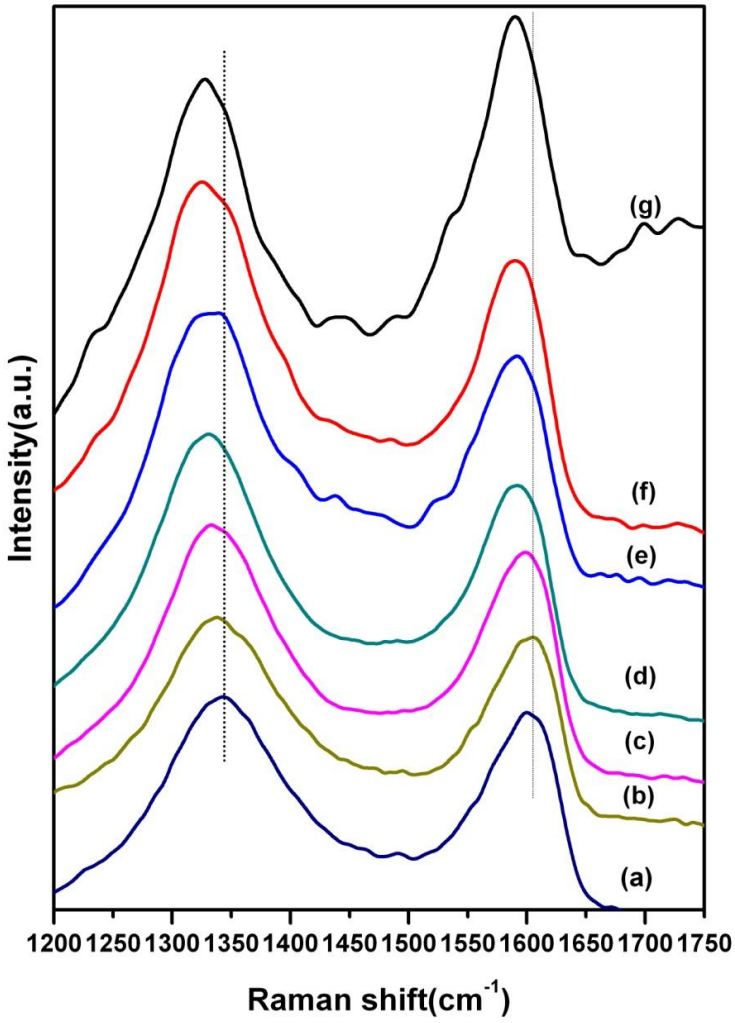

Figure 3.4(i) Raman spectra of Graphite oxide mixed with Lysine with varying concentrations. In spectras a to g the concentration of lysine with fixed concentration of GO are 1 mM, 1 mM, 10 mM, 50 mM, 100 mM,500 mM respectively.

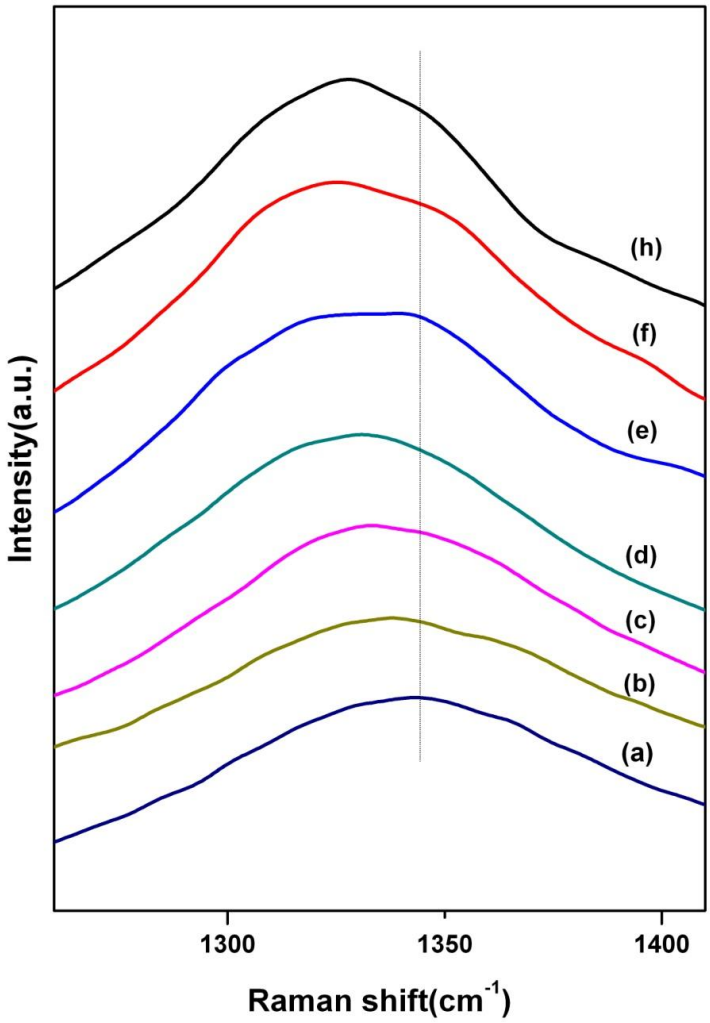

Figure 3.4(ii) The D bands of the samples. In spectras a to h the concentration of Lysine with fixed concentration of GO are 0.01 mM, 0.1 mM, 0.2 mM, 0.5 mM, 1 mM, 10 mM,100 mM respectively.

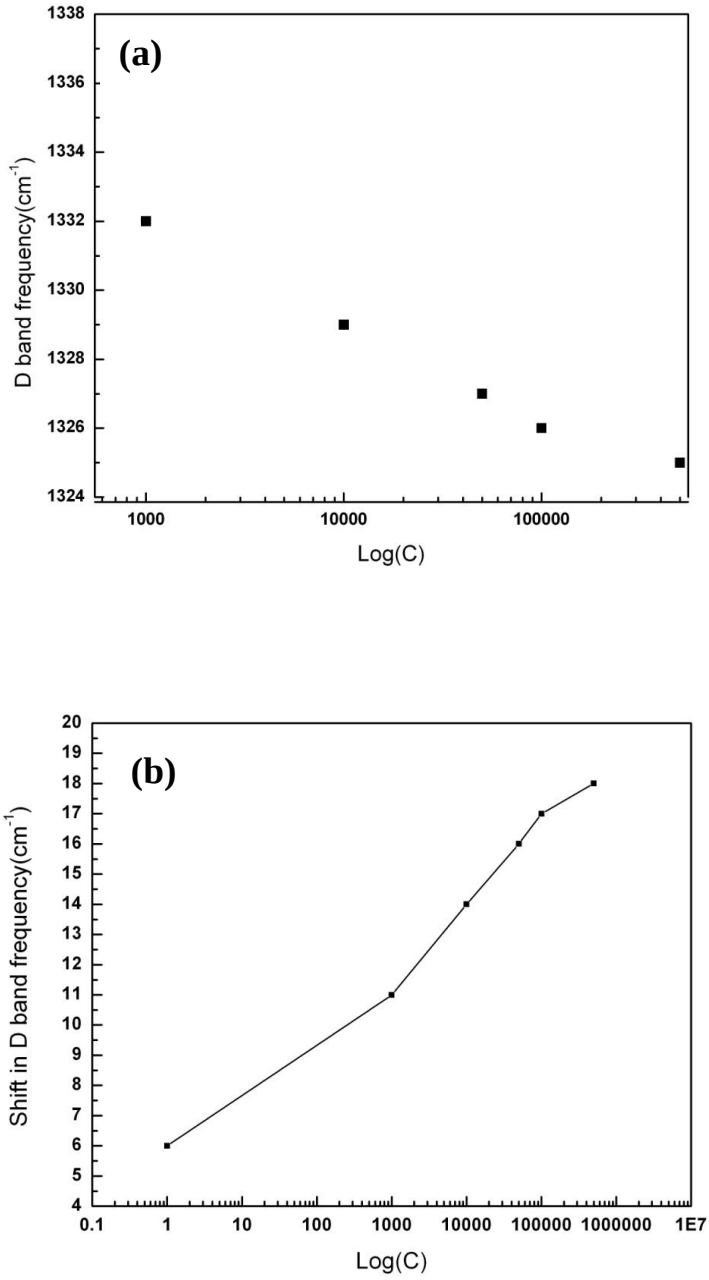

Figure 3.4(iii)(a) D band frequencies and (b) shift in D band frequencies at various concentrations of Lysine. Concentration C is in µM.

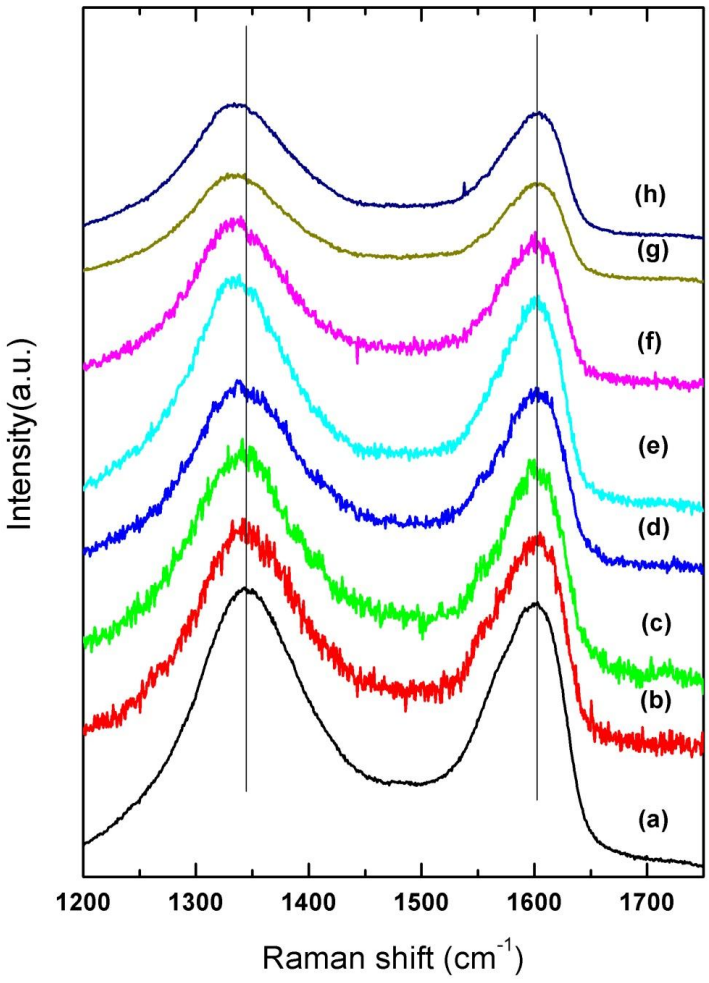

Figure 3.5(i) The Raman spectra of Graphite oxide mixed with aspartic acid with varying concentrations. In spectras a to h the concentration of aspartic acid with fixed concentration of GO are 0.01 mM, 0.1 mM, 0.2 mM, 0.5 mM, 1 mM, 10 mM,100 mM respectively.

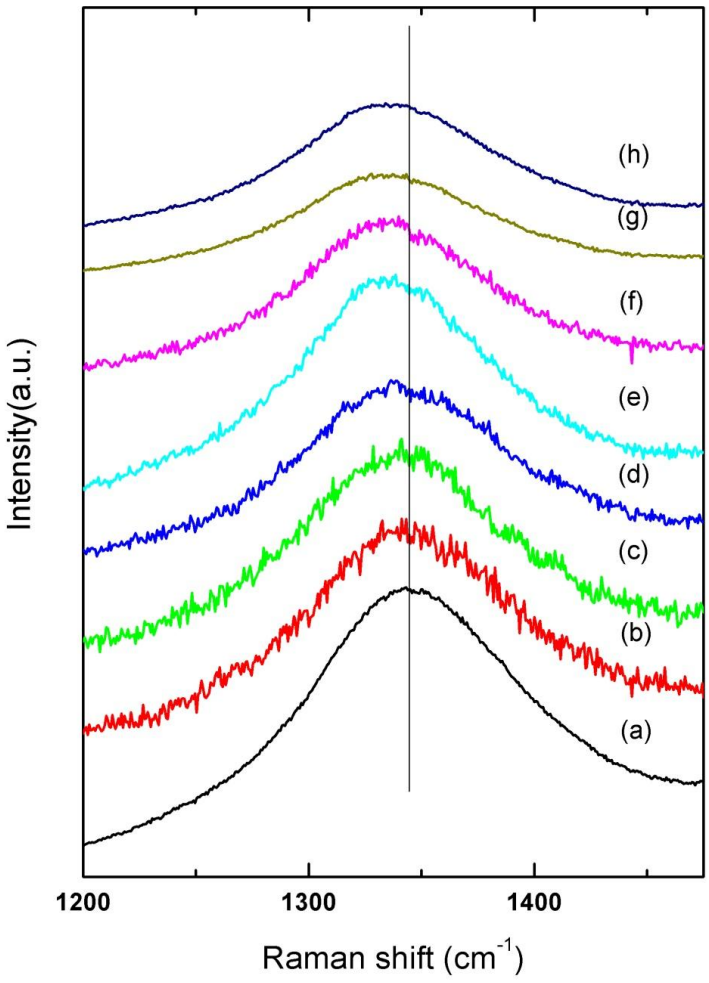

Figure 3.5(ii) The D bands of the samples. In spectras a to h the concentration of aspartic acid with fixed concentration of GO are 0.01 mM, 0.1 mM, 0.2 mM, 0.5 mM, 1 mM, 10 mM,100 mM respectively.

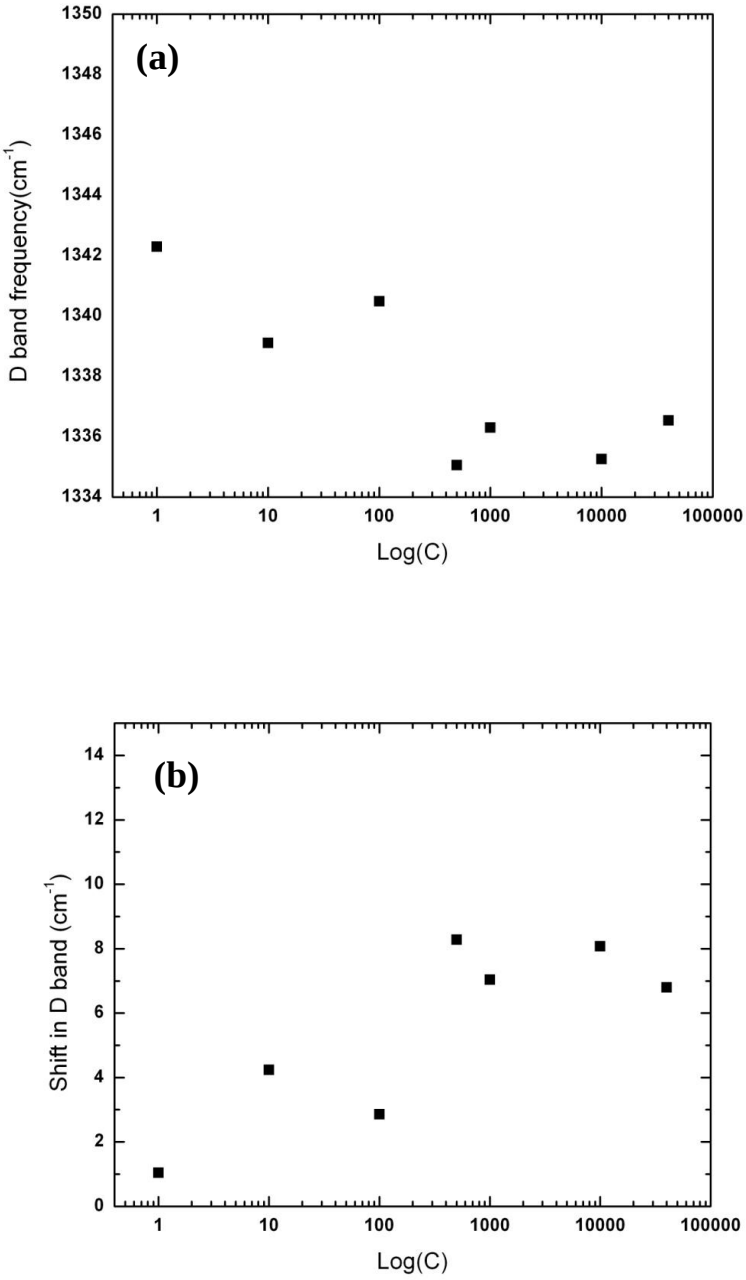

Figure 3.5(iii)(a) D band frequencies and (b) shift in D band frequencies at various concentrations of Lysine. Concentration C is in µM.

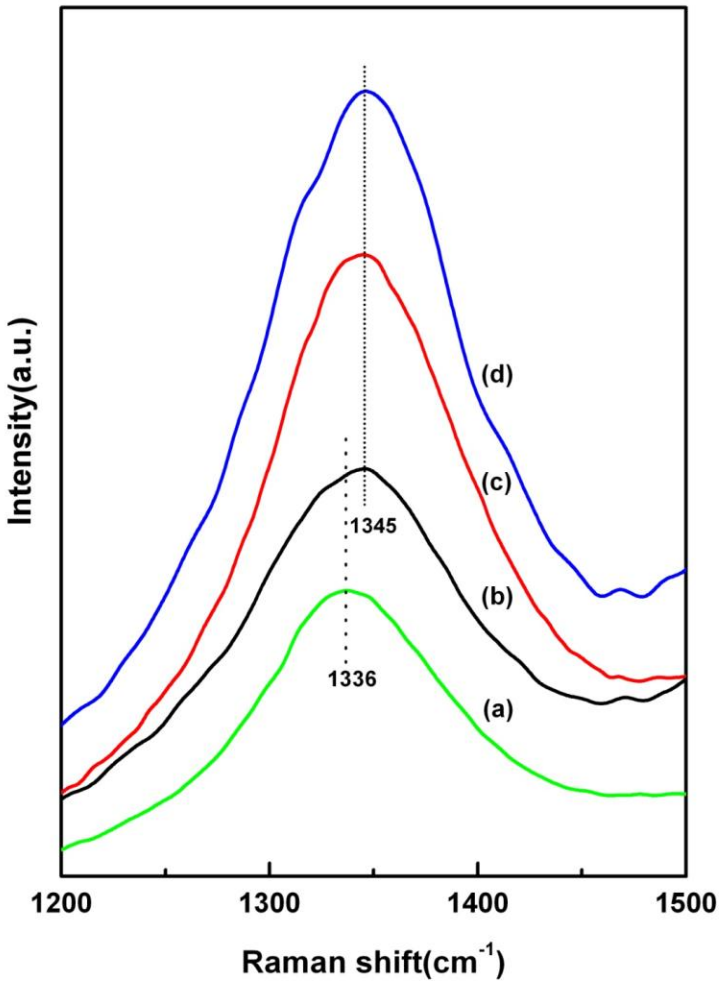

Figure 3.6(a) D band of GO+10 mM lysine before heating and (b) after heating at 350oC. (c) D band of GO before heating and (d) after heating

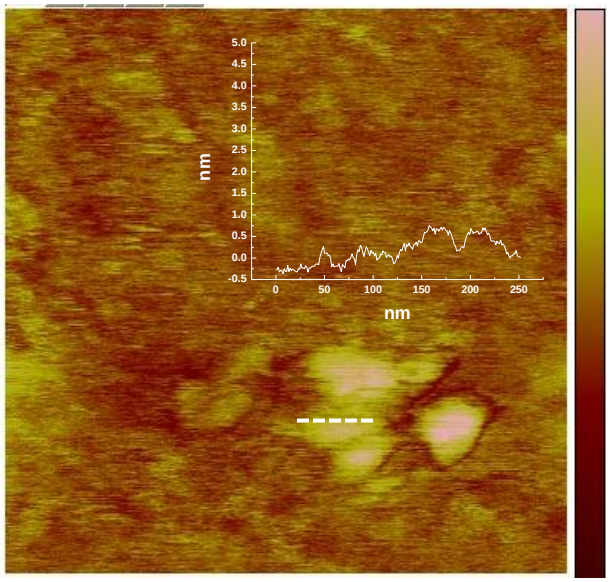

Figure 3.7 An AFM image showing a chemically synthesized graphite oxide flake

In order to verify if the nature of the molecule has any specific reason for the adsorption, we choose two amino acids both with positive and negative charges. From Figures 3.4 and 3.5 we see the same trend as observed with glucose in case of two amino acids lysine and aspartic acid. Lysine is a positively charged amino acid compared to aspartic acid is a negatively charged amino acid. On the other hand glucose is a neutrally charged molecule. Since graphite oxide is highly negatively charged, we get the largest shift in D band frequency for lysine than for aspartic acid and glucose. It is interesting to note that both the G and D band are affected in the case of Lysine, also the D band shifts below 1332 cm^{-1} to 1324 cm^{-1}, which could be because the Lysine not only is adsorbed on the oxygen rich parts, but also on other exposed parts of graphene. It is observed in the cases of amorphous carbon both the D band and G band appears much lower than the

diamond D band and graphite G band. In the case of Lysine too, the sp^2 character of the graphene is strongly affected due to the electrostatic interaction and charge transfer, causing an amorphous kind of resulting material at high concentration of Lysine. In the case of aspartic acid, due to the negative carboxylic group, the interaction between it and GO is more or less due to formation of hydrogen bonding and we observe that the effect is similar to the case of glucose which is neutral in charge.

For our studies we avoided using any electrolytes to prevent any surface charge alteration before adsorbtion of the analyte molecules. It is also evident that this kind of molecular interaction is indeed adsorbtion. This can be ascertained from the fact that upon heating the system to about 350 ^{o}C the D band comes to the original position similar to that of before adsorbtion (Figure 3.6). Now the question arises that why there is a shift in the D band of graphite oxide? Both D and G' bands are related to non-zone-center phonons, and the dispersive behaviour is explained by a double-resonance Raman process [13]. The variation in D and G' band frequencies obtained with the same laser energy for different carbon materials is due to the slightly greater force constants for more well ordered carbon atoms[14]. In case of adsorbtion of molecules to the Graphite oxide flakes, the force constants of the bond changes due to the hydrogen bonding to the polar oxygen groups. Since, on formation of hydrogen bond with the atoms, the effective force constant decreases, keeping the mass constant and hence, the frequency changes to lower values. Considering the double resonance process (Figure 3.8) two scattering occurs, one at the k point called the intra-valley scattering and another scattering takes the electron

from k to k’ which is called an inter-valley scattering process. The D band (which involves one phonon and one elastic scattering events) and the G’ band (which involves two phonons) are both inter-valley scattering processes, and thus the corresponding phonons are K point iTO phonon modes[13]. Due to hydrogen bonding, the effective force constant changes leading to the change in TO phonon frequency. Therefore the D band frequency which is a sum of the phonon frequency and the elastic scattering has a lower value leading to a lower frequency.

We had also tried to adsorb gold atoms on the GO. We avoided nanoparticles, as they generally have a capping agent which could interfere with our results. It has been reported that gold atoms bind preferentially to the defect sites of carbon nanotubes[15]. So, we tried to sputter gold atoms onto the graphite oxide flakes. But in this case we failed to observe any D band frequency shift. The reason for this is that merely nucleation is not sufficient for this shift but some kind of stronger electrostatic interaction or hydrogen bonding is necessary to bring about this shift. The attachment of the molecules to the GO backbone increases the sp^3 character of the system, which affects the D band.

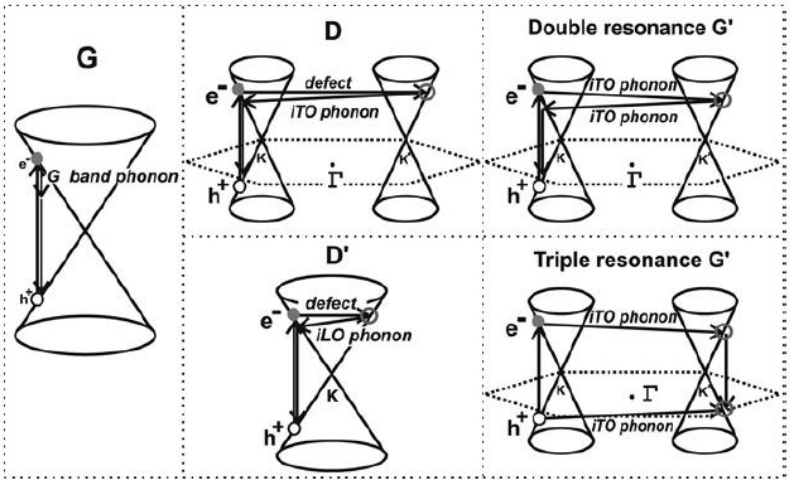

Figure 3.8 The first and second order double and triple resonance processes which are responsible for the various bands in graphene

Therefore, we see that physical adsorption of molecules to the defect sites indeed is the cause of the shift of the D band of the graphite oxide. This process can be exploited for the detection of small molecules which interacts with the graphite oxide and can be helpful for the sensing of molecules in an easy and effective manner.

3.4 Conclusion

We have shown that small molecules sensing using graphite oxide flakes is possible from the D band shifts caused by physical adsorbtion of the molecules. Further

studies are being conducted to see whether this method can be used to observe the level of sugar in the blood or for the quantitative detection of glycated haemoglobin in blood and also detection of other biologically relevant molecules.

3.5 References

[1] E. S. Snow, F. K. Perkins, E. J. Houser, S. C. Badescu, T. L. Reinecke, *Science* **2005**, *307*, 1942.

[2] E. S. Snow, F. K. Perkins, *Nano Letters* **2005**, *5*, 2414.

[3] G. Lu, L. E. Ocola, J. Chen, *Nanotechnology* **2009**, *20*, 445502.

[4] E. Bekyarova, I. Kalinina, M. E. Itkis, L. Beer, N. Cabrera, R. C. Haddon, *Journal of the American Chemical Society* **2007**, *129*, 10700.

[5] J. A. Robinson, E. S. Snow, S. C. Badescu, T. L. Reinecke, F. K. Perkins, *Nano Letters* **2006**, *6*, 1747.

[6] G. H. Lu, L. E. Ocola, J. H. Chen, *Applied Physics Letters* **2009**, *94*.

[7] I. Jung, D. Dikin, S. Park, W. Cai, S. L. Mielke, R. S. Ruoff, *Journal of Physical Chemistry C* **2008**, *112*, 20264.

[8] J. T. Robinson, F. K. Perkins, E. S. Snow, Z. Q. Wei, P. E. Sheehan, *Nano Letters* **2008**, *8*, 3137.

[9] P. Ramesh, S. Bhagyalakshmi, S. Sampath, *Journal of Colloid and Interface Science* **2004**, *274*, 95.

[10] A. Gupta, G. Chen, P. Joshi, S. Tadigadapa, Eklund, *Nano Letters* **2006**, *6*, 2667.

[11] L. G. Cantado, M. A. Pimenta, B. R. A. Neves, M. S. S. Dantas, A. Jorio, *Phys. Rev. Lett.* **2004**, *93*, 247401.

[12] A. C. Ferrari, J. Robertson, *Phys. Rev. B* **2000**, *61*, 14095.

[13] L. M. Malard, M. A. Pimenta, G. Dresselhaus, M. S. Dresselhaus, *Physics Reports* **2009**, *473*, 51.

[14] M. J. Matthews, M. A. Pimenta, G. Dresselhaus, M. S. Dresselhaus, M. Endo, *Phys. Rev. B* **1999**, *59*, R6585-R6588.

[15] I. Suarez-Martinez, C. Bittencourt, X.Ke, A. Felten, J.J. Pireaux, J. Ghijsen, W. Drube, G. van Tendeloo, C.P. Ewels, *Carbon***2009**, *47*, 1549.

Chapter 4

Formation of nanoparticle arrays and multifunctional nanostructures for SERS

4.1 Motivation

Formation of nanostructures of different shapes and sizes or arranged in various configurations has gained a lot of scientific interests. The miniaturization of devices or building sensors of high sensitivity requires techniques which depends on the shape, size and arrangement of nanoparticles in 1D, 2D or 3D arrangements. A technique like SERS, which uses these kinds of nanoparticle arrangement, has been predicted to be the next big revolution in the field of bio diagnostics[1].

Nanoparticles of metals, semiconductors and quantum dots have received much attention due to their different properties at nanoscale than bulk. Gold and silver nanoparticles are now the most studied because of their applications in electronics[2], sensors[3, 4], catalysis[3] and bio labeling. It is necessary to control the size and shape of the monodispersed particles in order to obtain nanoparticles with desired properties. It is a challenge to arrange nanoparticles on desired regions selectively. In order to obtain a locally arranged pattern with nanoparticles there are top down or bottom up approaches like the e-beam lithography[5], microcontact printing[6], UV photolithography[7] etc.

S. Mohapatra, S. Siddhanta, C. Narayana, T. Maji, "A facile bottom up approach for fabricating multifunctional silver nanorods", Journal of Material Chemistry 2010(submitted).

Nanoparticles can be allowed to self assemble on a selective region by nanoimprint lithography[8].

In this chapter we have shown how the 3D assembly of silver nanorods and rod-like linear arrays of gold nanoparticles are candidates for SERS of analyte molecules.

4.2 Materials and methods

4.2.1 Silver nanorods

The silver nanorods were prepared by the method described elsewhere. For SERS with silver nanorods, molecules were adsorbed onto the nanoparticles by dropping 1 μL of 1 mM of Thiophenol (TP) in ethanol followed by drying. Excess unadsorbed molecules were washed off with ethanol. For concentrations of micromolar and pM, the nanoparticles and the solution were mixed and sonicated for 15 minutes prior to dropping on the glass substrate.

4.2.2 Gold nanoparticles array

For formation of gold nanoparticles array the gold nanoparticles were embedded into microtubes formed from 1-hydroxybenzotriazole (HOBT), a small heterocyclic molecule. Gold nanoparticles were prepared by the Lee and Meisel method. An aqueous

mixture (1:1, v/v) of HOBT (2 mg/mL) and gold nanoparticles solution (GNP's)(8-10 nm)(10^9 to 10^{12} particles/mL) were sonicated and evaporated at 18 ^oC. The HOBT microtubes containing GNP's were melted at 140 ^oC for 10 minutes. For labelling the GNP's with R6G an aqueous mixture (1:1:1 v/v/v) of the GNP's (10^{12} particles/mL), HOBT (2 mg/mL) and R6G (0.1 mM), were evaporated on silicon wafer at 18 $^oC$and were heated at 140 ^oC for 10 minutes to yield microtubes.

4.3 Results and discussions

4.3.1 SERS with silver nanorods

UV visible spectrum of the silver nanorods (see Figure 4.1) prepared shows two surface plasmon resonance band one at 420 nm and second weaker band at 736 nm due to structural anisotropy. The silver NRs have a tendency to agglomerate over time. Hence, if one incubates the absorbate with the silver NRs and allows them to agglomerate it is possible to form hotspots which trap these absorbates. These hotspots can also be produced by repeated washing with methanol which makes the silver NRs to agglomerate and form larger structures as shown from FESEM pictures (Figure 4.4) and UV-visible spectra (Figure 4.2). The inset in Fig. 4.4 shows places where these hot spots exist. If this is true then we must expect a large SERS enhancement. We have taken thiophenol (TP) as the test molecule and Fig. 4.3 shows the SERS spectra of TP obtained by repeatedly

washing the Ag nanorods and incubating it with TP, which is deposited on a glass substrate.

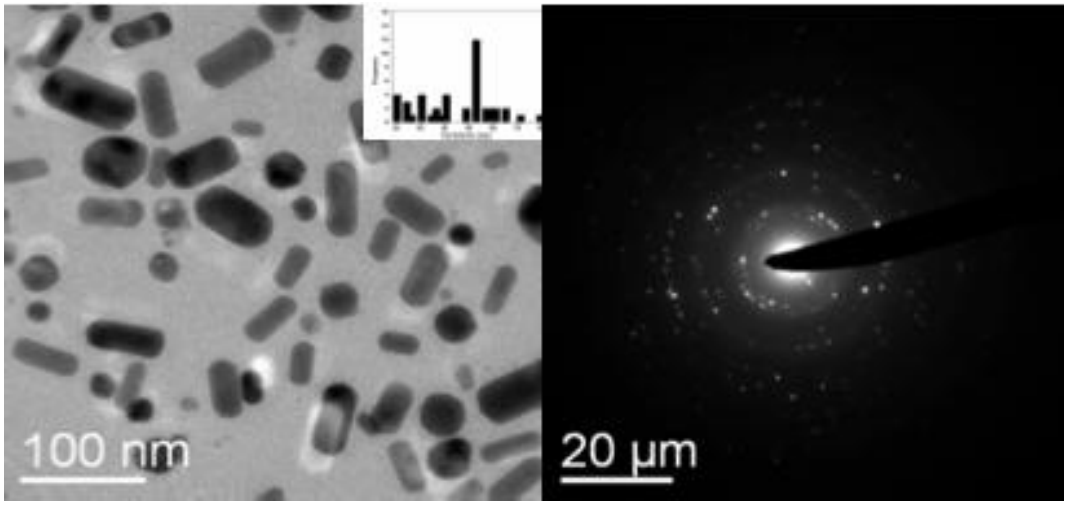

Figure 4.1 TEM figure of the gold nanorods and the corresponding Electron diffraction pattern

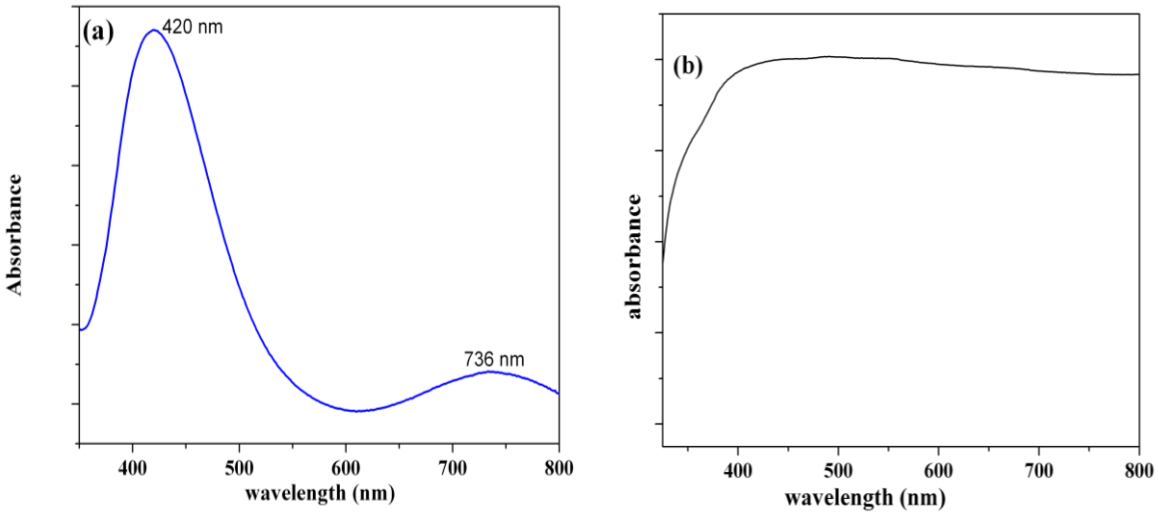

Figure 4.2 Uv-vis spectra of the nanorods (a)before and (b) after wash with methanol

The spectral features agree well with the reported values. The enhancement factor G was calculated by the procedure given by Yu et al[9]

$$G = (I_{SERS}/I_{norm})(N_{bulk}/N_{surf})$$

where I_{SERS} and I_{norm} are the intensities of a specific band in SERS and normal Raman of test molecule, respectively. N_{bulk} and N_{surf} are the number of probe molecules under laser illumination in the bulk and SERS experiments, respectively. We have chosen two bands at 1069 cm^{-1} and 1572 cm^{-1} to calculate G factor for TP. N_{surf} is given by CA, where C and A are surface densities of TP (6.8 X 10^{14} molecules cm^{-2}) and area of the laser spot on the sample, respectively[10]. On the other hand, N_{bulk} is given by $N_{bulk} = Ah\rho/m$, where *h*, ρ and *m* are the penetration depth (100 μm), the density (1.079 g cm^{-1}), and the molecular weight 110.18 g mol^{-1} of TP. In the present experiment, we obtained the G ~ 10^5 for TP.

We also observed that for molecule like R6G and TP, we can detect these molecules at pM concentrations and in the case of phenylalanine we could go down to μM concentration as shown in the inset of Figure 4.3. Sun et al have reported that dissolution of capping agents like CTAB in ethanol results in formation of aggregates[11]. Chen et al have shown that the electromagnetic enhancement depends strongly on the degree of aggregation of silver nanoparticles[12]. 3-D aggregation of nanoparticles strongly influences the SERS enhancements as shown by Pignataro et al[13]. Many a times for stronger SERS signals aggregating agents like NaCl, KCl, KNO_3

are used[14]. In our case washing with methanol reduces the density of capping agents on the NR surface facilitating the adsorbates to be adsorbed on to the surface. The reduction in the capping agents facilitates creation of 3-D structures with hotspots. The broad UV-visible spectra Figure 4.2(b) shows this. The advantage of a nearly flat response in UV-visible spectra is that there is no restriction on the excitation source to be used for SERS. To demonstrate this we have chosen an excitation source 632.8 nm, which is far away from the UV-Visible absorbtion peak of 416 nm and 736 nm for single silver NR and we demonstrate a strong SERS ($G \sim 10^5$).

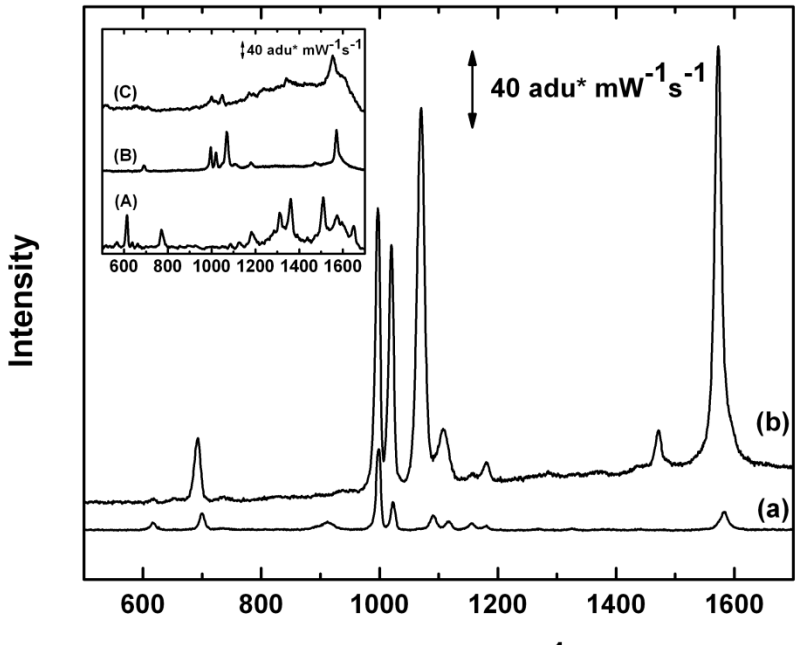

Figure 4.3 SERS spectra of Thiophenol(TP) (a) without and (b) with nanoparticles (Inset) SERS spectra of (a) Rhodamine 6G(R6G, 1 pM), (b)Thiophenol(TP, 1pM) and (c) Phenylalanine(1 micromolar)

It is known that in case of aggregated nanoparticles the energy from the excitation source is not distributed uniformly over the nanoparticles but is localized in small areas called “Hot Spots”[15]. Molecules trapped in these hotspots experience enhanced optical field which leads to electromagnetic enhancements. These hotspots are responsible for extraordinary Raman signal enhancement in single molecule experiments. These are shown in the inset of the FESEM image of the agglomerated NRs shown in Figure 4.4. The NRs aggregate in form of 2-D chains as well as 3-D agglomerates. These hotspots provide the ability to detect pM concentration of analytes.

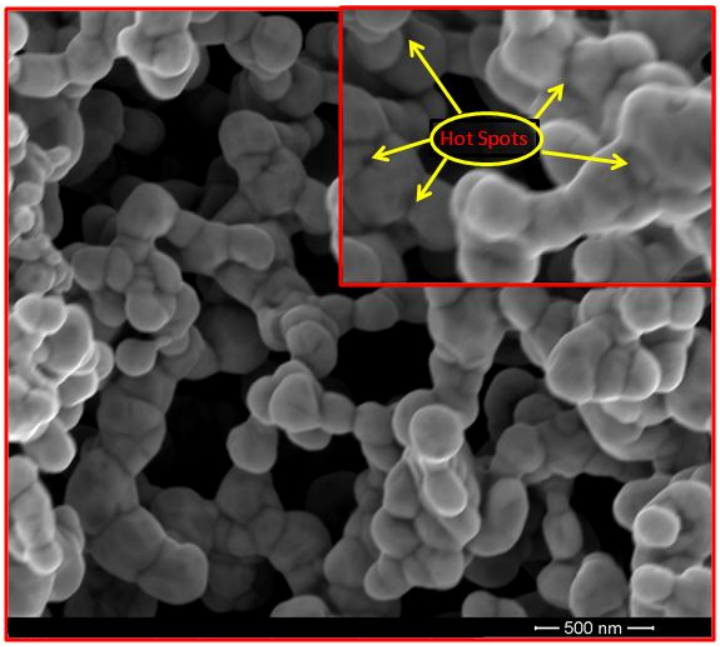

Figure 4.4 The 3-dimensional aggregation of the silver nanorods. The inset shows the hotspots present.

The spectral features of TP, R6G and phenylalanine obtained are similar to earlier reports[16-18]. It should be noted that in the case of R6G there is some background fluorescence observed, which has been subtracted for clarity. The presence of fluorescence shows that R6G is not strongly adsorbed and is not chemically bonded to the surface of the NRs. In the case of thiophenol, the thiol group helps in chemical binding leading to no residual background giving rise to stable SERS spectra. The large decrease of frequency of the in-plane breathing mode coupled to the υ_{C-S} mode from 1092 cm^{-1} to 1069 cm^{-1} in the SERS spectra show that the TP molecule is bonded to the metal surface[19]. Hence the present NRs have a preference on the types of analytes which it can be used to detect. The presence of groups containing sulphur, π electrons and nitrogen facilitates chemical binding or strong adsorption on these NRs resulting in its ability for trace detection.

4.3.2 SERS with gold nanoparticles array

HOBT (Figure 4.5) can serve as new self assembling building block for the synthesis of advanced organic and hybrid materials which can be used as containers for nanoreactors. In this study GNP's have been incorporated into the hollow cavities of HOBT microtubules which upon heating yield microrods with smooth surface and high morphological purity. R6G chromophore labeled gold microarrays has been synthesized which exhibited characteristic SERS acitvity.

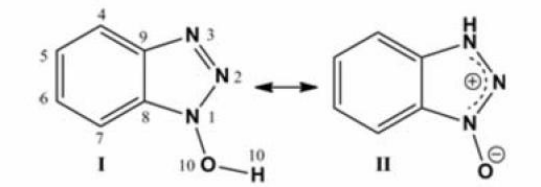

Figure 4.5 The two tautomeric structures of 1- hydroxybenzotriazole(HOBT)

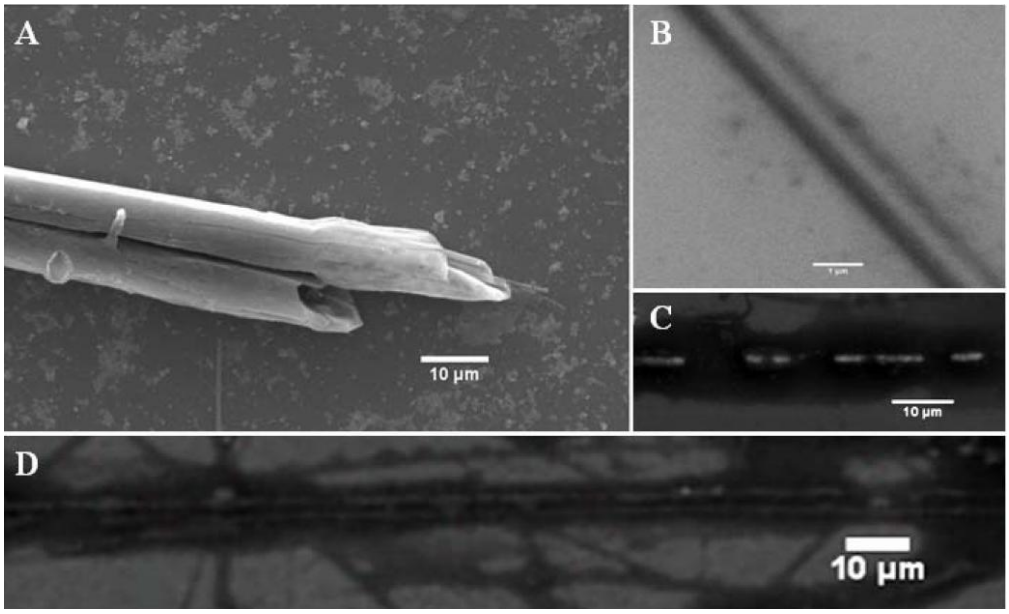

Figure 4.6 Synthesis of rod-shaped gold nanoparticles array: A)High resolution SEM (HR-SEM) image of a pair of closely self-assembled, well-separated open-ended microtubular structures synthesized by evaporation of a sonicated aqueous mixture (1:1 v/v) of HOBT (1 mg/mL) and GNPs (10^{10} particles/mL) (8-10 nm diameter). B) Magnified SEM image of a portion of a gold microrod with smooth surface. C) Discontinuous sausage like linear arrays of gold microrods with uniform diameters. D) A pair of closely aligned well-separated gold microwires. Melted HOBT is seen as dark patches around the linear gold microrods in images C & D.

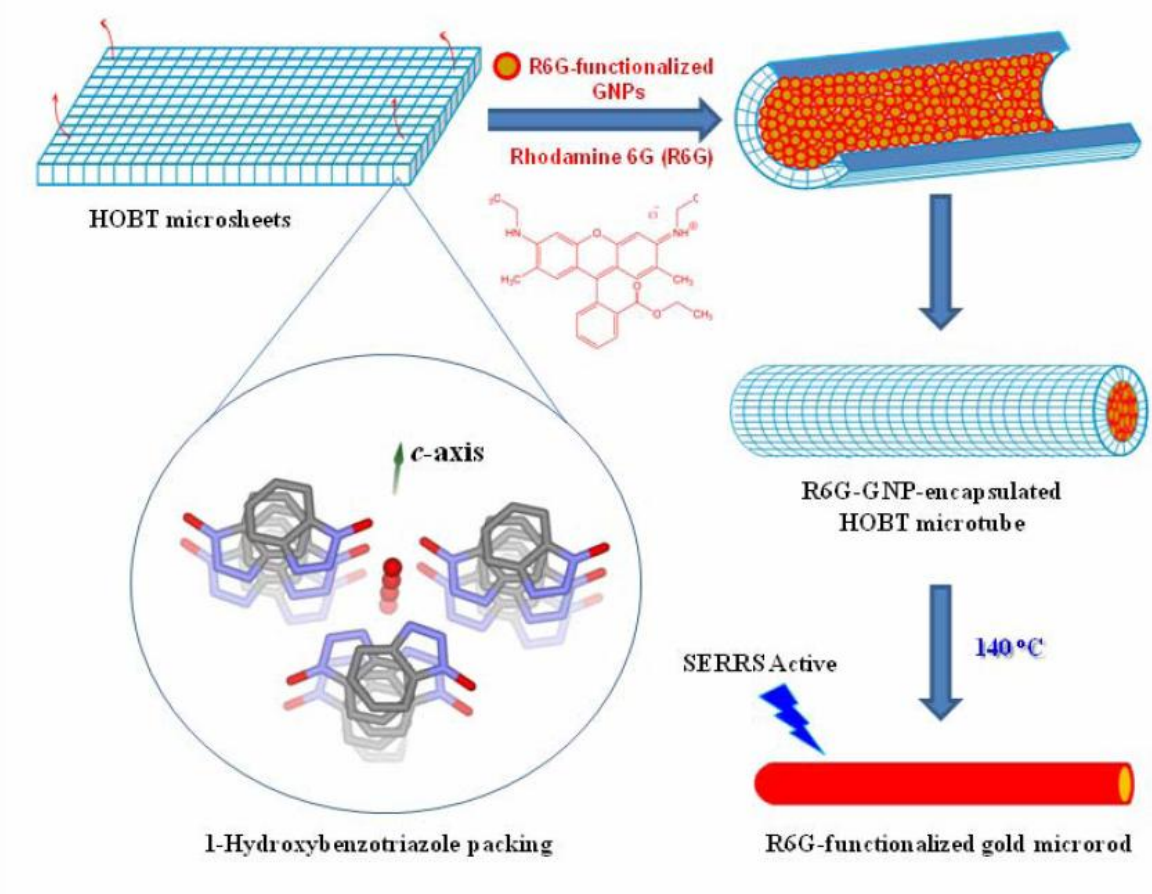

Figure 4.7 Mechanism of self assembly of HOBT and formation of rod-like gold nanoparticles array

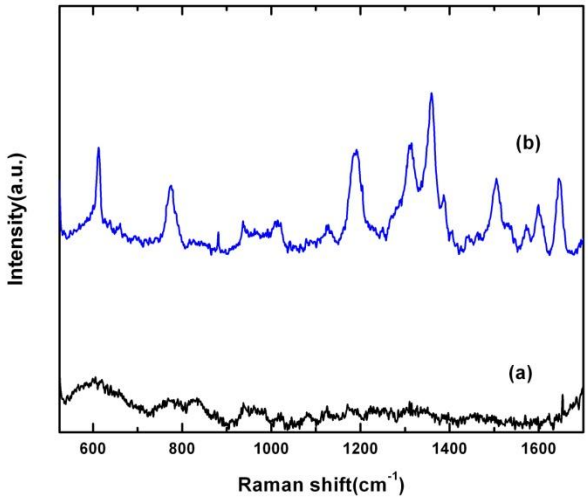

Figure 4.8 (a)Raman spectra of gold microrods without R6G, (b)SERS spectra of R6G labelled gold microrods.

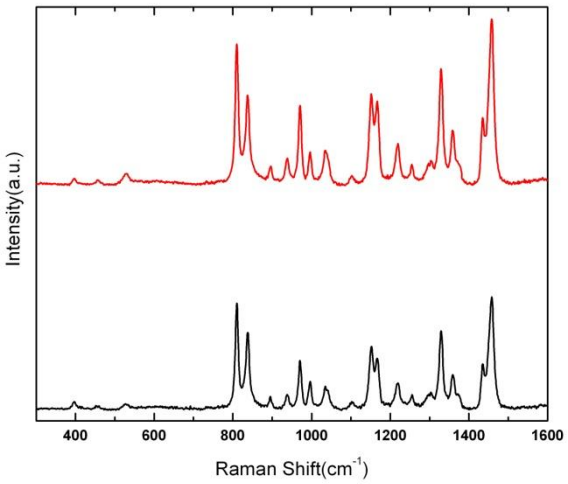

Figure 4.9 SERS spectra of: (red) HOBT in water (2mg/mL) and (blue) a mixture (1:1, v/v) of HOBT (2 mg/mL) and GNPs (1010 particles / mL) in water. There is no enhancement or modification of the Raman bands of HOBT upon mixing with GNPs (10^{8}-10^{12} particles / mL) in aqueous solution.

Figures 4.6 shows the SEM images of the HOBT microtubules and Fugure 4.7 shows the mechanism of formation and encapsulation of GNP's. Figure 4.8a shows that there is no signal from the gold microrods without the presence of analytes. This is also due to the fact that the HOBT molecules don't preferably bind to the gold nanoparticles, which is evident from the spectra shown in Figure 4.9. If the GNP's interacted with the HOBT molecules, there had been an enhancement in SERS spectra which is not seen in this case. The gold nanoparticles which were tagged with R6G dye molecules showed SERS signal after they were exposed by melting the microtubules (Figure 4.8b). Therefore we can see that this method of encapsulation and formation of nanoparticles arrays and nanorods can be used as an alternative method for lithography to form this kind of nanostructures on different surfaces.

4.4 Conclusion

We have shown that silver nanorods can be assembled in three dimensional arrays with hotspots which give a detection of very low concentrations of the analyte. We have also shown that gold nanoparticles can be encapsulated in an organic microtubule to form a gold microrod which is SERS active. This open up the possibility of encapsulating SERS active materials into structures which can act as containers and which can release these materials at the desired places and at the desired environment.

4.5 References

[1] N. L. Rosi, C. A. Mirkin, *Chemical Reviews* **2005**, *105*, 1547.

[2] B. R. Cuenya, S. H. Baeck, T. F. Jaramillo, E. W. McFarland, *Journal of the American Chemical Society* **2003**, *125*, 12928.

[3] D. T. Thompson, *Nano Today* **2007**, *2*, 40.

[4] F. J. Hernandez, S. K. Dondapati, V. C. Ozalp, A. Pinto, C. K. O'Sullivan, T. A. Klar, I. Katakis, *Journal of Biophotonics* **2009**, *2*, 227.

[5] J. P. Spatz, V. Z. H. Chan, S. Mossmer, F. M. Kamm, A. Plettl, P. Ziemann, M. Moller, *Advanced Materials* **2002**, *14*, 1827.

[6] S. H. Yun, B. H. Sohn, J. C. Jung, W. C. Zin, M. Ree, J. W. Park, *Nanotechnology* **2006**, *17*, 450.

[7] B. Gorzolnik, P. Mela, M. Moeller, *Nanotechnology* **2006**, *17*, 5027.

[8] J. P. Lee, E. U. Kim, H. D. Koh, N. G. Kang, G. Y. Jung, J. S. Lee, *Nanotechnology* **2009**, *20*.

[9] H. Z. Yu, J. Zhang, H. L. Zhang, Z. F. Liu, *Langmuir* **1998**, *15*, 16.

[10] A. D. McFarland, M. A. Young, J. A. Dieringer, R. P. Van Duyne, *The Journal of Physical Chemistry B* **2005**, *109*, 11279.

[11] L. Sun, Y. Song, L. Wang, C. Guo, Y. Sun, Z. Liu, Z. Li, *The Journal of Physical Chemistry C* **2008**, *112*, 1415.

[12] M. C. Chen, S. D. Tsai, M. R. Chen, S. Y. Ou, W. H. Li, K. C. Lee, *Phys. Rev. B* **1995**, *51*, 4507.

[13] B. Pignataro, A. De Bonis, G. Compagnini, P. Sassi, R. S. Cataliotti, *Journal of Chemical Physics* **2000**, *113*, 5947.

[14] O. K. Song, M. A. Pauley, C. H. Wang, A. K. Y. Jen, *Journal of Raman Spectroscopy* **1996**, *27*, 685.

[15] E. C. Le Ru, P. G. Etchegoin, *Chemical Physics Letters* **2004**, *396*, 393.

[16] K. T. Carron, L. G. Hurley, *The Journal of Physical Chemistry* **1991**, *95*, 9979.

[17] J. A. Dieringer, K. L. Wustholz, D. J. Masiello, J. P. Camden, S. L. Kleinman, G. C. Schatz, R. P. Van Duyne, *Journal of the American Chemical Society* **2008**, *131*, 849.

[18] S. Stewart, P. M. Fredericks, *Spectrochimica Acta Part A: Molecular and Biomolecular Spectroscopy* **1999**, *55*, 1641.

[19] M. A. Bryant, S. L. Joa, J. E. Pemberton, *Langmuir* **1992**, *8*, 753.

Chapter 5

Incorporation of silver chloride and silver nanoparticles in bacterial cellulose membranes

5.1 Motivation

A wide variety of materials from organic, inorganic to biological are nowadays used in synthesis and fabrication of various types of nanoparticles with unique shapes and properties. Biological materials and organisms are interesting templates for growth and assembly of nanoparticles. Biopolymers such as DNA[1-3], RNA[4, 5] and proteins[6] have been used as templates for the synthesis and organization of metal and semiconductor nanoparticles. Bacterial[7], virus[8, 9], yeast[10] and fungi[11] are used for similar purposes. The biological templates are useful because of their precise structures and spatial organization they impart on the nanostructures, as well as specific affinities for binding to surfaces and nucleating and assembling certain materials[12].

Bacterial cellulose (BC), produced by acetobacter is one of the templating materials with several unique properties. Some of its properties are high porosity, water absorbance, mechanical properties and biocompatibility [13, 14]. BC has nano porous three-dimensional network structure, high surface area and presence of high density of hydroxyl and ether groups, which allows formation and growth of nanostructures in it.

A manuscript is under preparation based on the work done in this chapter.

Also BC has good water adsorbtion properties and swelling characteristics on adsorbtion of water. Because of the water adsorbtion property, it is easy to sterilize it and attain high chemical purity without any change in the structure. This makes it ideal for its use as as wound dressing as well as environment friendly food packaging material. Incorporating various oxide and noble metal nanostructures into BC can lead to multifunctional materials with a variety of uses.

Incorporation of silver and oxide nanoparticles like copper oxide can make these membranes antimicrobial and antibacterial[15] and therefore can be used as bandages and food packaging materials. The antimicrobial property of silver is well studied and is of great importance because of its ability to inhibit the growth or cell disruption of bacteria and inactivation of other eukayotes. Also self sustained, biodegradable and biocompatible films containing noble metal nanoparticles has been fabricated for potential application in nanobioscience and ultrasensitive chemical and biochemical analysis. Gold and silver nanoparticles can be incorporated into BC to fabricate SERS substrate for analysis of trace molecules[16].

In our earlier work a nanocomposite was made of silver nanoparticles and bacterial cellulose by using hydrazine as a reducing agent. It showed optimal growth inhibition property against *Staphyloccus aureus* and this effect was more than that observed with sodium borohydride reduced nanocomposite. But one of the drawbacks of this process is that the sizes of the nanoparticles could not be controlled in an efficient manner because of which it was not possible to use it as a SERS substrate. In the present

work we have shown the possibility to control the surface coverage as well as the size of the nanoparticles incorporated into cellulose matrix using a green method of synthesis which do not use harmful chemicals like hydrazine and sodium borohydride. Also being biocompatible with no traces of harmful chemicals it has dual advantages. A substrate for SERS as well as an antibacterial material. In this work we have incorporated silver chloride nanocrystals in the bacterial cellulose paper and reduced it using the novel and green chemistry of sodium sulfite using ascorbic acid as an inductor. Another method in which silver ions were reduced by ferrous ions in presence of acetic acid was also used.

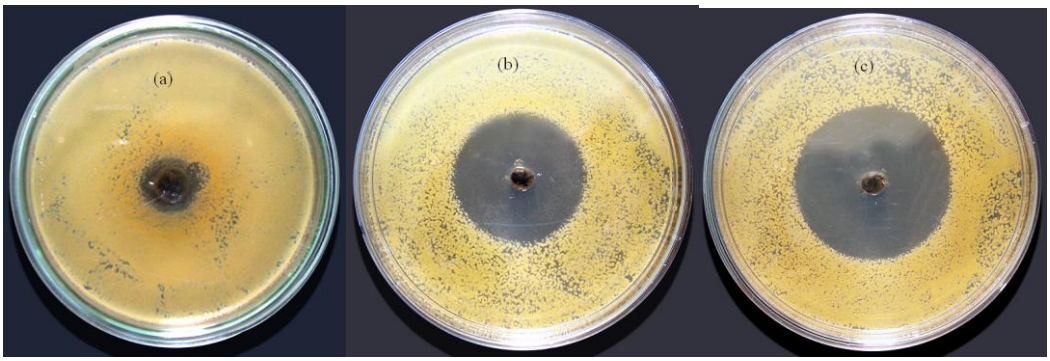

Figure 5.8 Antibacterial efficacy of (a) papain treated BC- silver Nanocomposite(NC) obtained by reduction of silver nitrate with hydrazine, (b) papain treated BC-silver NC obtained by reduction of silver nitrate with sodium borohydride and (c) NaOH treated BC-silver NC obtained by reduction of silver nitrate with hydrazine, respectively[17].

5.2 Materials and methods

5.2.1 Chemicals

All the chemicals, silver nitrate (Spectrochem India Pvt. Ltd., 99.8%), Ascorbic acid (Ranbaxy, India), sodium hydroxide (Merck, ≥ 97%), Sodium sulfite (SD-fine chem., India) and Sodium Chloride (Merck) were used without further purification. Brain heart infusion broth, tryptic soy agar broth and agar used in the media preparation for bacterial growth and antibacterial evaluation were obtained from Hi-Media Lab. Pvt. Ltd., Mumbai, India. Millipore water was used for all washing procedures as well as solutions preparation.

5.2.2 Preparation of NaOH treated Bacterial Cellulose(BC)

Acetobacter xylinium was used for the biosynthesis of BC under static culture conditions at 25-35 ^{o}C as described in our earlier work[18]. The paper matrix was treated with 0.2 M boiling NaOH solution for 15-20 min, to remove the matrix proteins and other cell debris. The matrix was further washed with 250 mL of distilled water for 2-3 times and then compressed and dried between filter papers.

5.2.3 Incorporation of Silver Chloride

Silver nitrate solutions of concentrations 100 mM, 10 mM, 1 mM and 0.1 mM were prepared in water. Sodium chloride solutions of concentrations 100 mM, 10 mM, 1 mM and 0.1 mM were also prepared in water. The bacterial cellulose paper was cut into pieces of 1 cm^2 area and dipped in silver nitrate solution (2 mL) for 4 hours. After drying the paper on filter paper, it was dipped into the same concentration of sodium chloride solution (2 mL) for 4 hours. This process was repeated 5 times. All the reactions were done in dark to avoid photoreduction. The paper was then washed with water and characterized.

5.2.4 Reduction of Silver Chloride

25 mL of reaction mixture containing 1 µM of ascorbic acid and 5 µM of sodium sulfite was prepared in water. The silver chloride nanoparticles incorporated was immersed in this solution in dark for 4 hours.

5.2.5 Reduction of Silver ions using ferrous ions

The bacterial cellulose paper was cut into area of 1cm^2 and was dipped into 0.2 M NaOH solution for 12 hours. The paper was washed with ethanol and dried on filter

paper. The paper was then dipped into 100 mM of silver nitrate solution for 12 hours. The paper was then washed with ethanol to remove excess of silver ions. The paper was then dipped into 2 mL of reaction mixture containing 5 mM ferrous chloride and 20 mM acetic acid.

5.2.6 Measurements

Uv-vis absorption measurements were done by using a Perkin-Elmer Lambda 900 UV/VIS/NIR spectrophotometer. Field Emission Scanning Electron Microscopy (FE-SEM) was done by using a Nova 600 NanoSEM (FEI, Germany). The composition mainly carbon, oxygen and silver of NC were determined by using EDAX equipped in the FE-SEM. All the measurements were performed at room temperature (298 K). XRD measurements were done using a Bruker D8 discover instrument using Cu-Kα radiation.

5.3 Results and discussions

Figure 5.1 shows the FESEM images of the AgCl nanocrystals formed on the bacterial cellulose at different concentrations. As the concentration of silver nitrate was increased the surface coverage of these nanocrystals increased considerably as evident from the images. Also the size distribution of the nanoparticles is very broad from around

20 nm to a several tenths of nanometers. This is probably because new nanocrystals were formed at each dipping step and the previously formed ones increased in size.

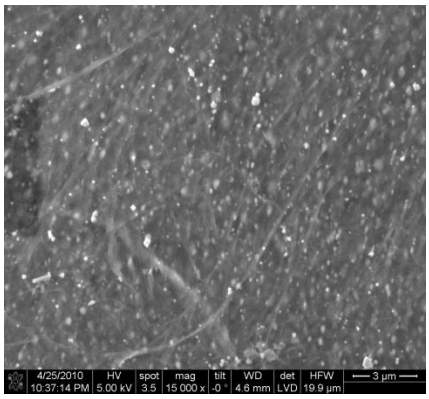

(a)

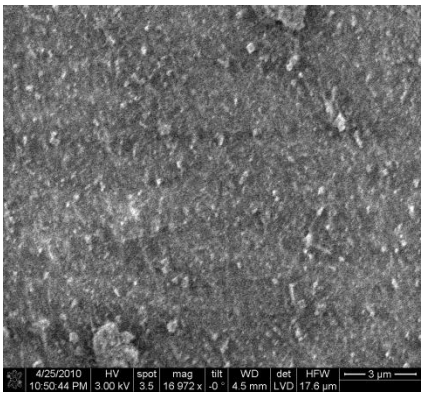

(b)

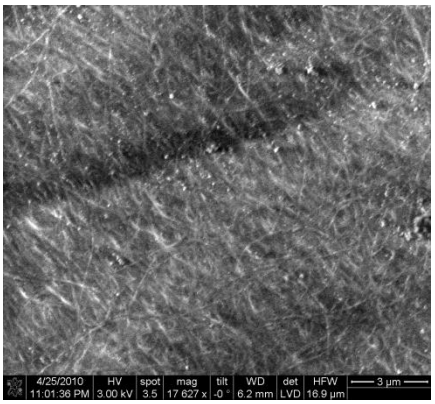

(c)

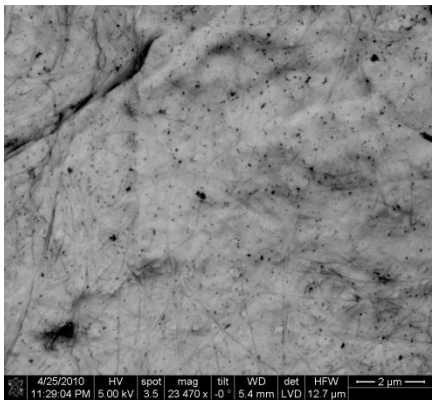

(d)

Figure 5.9 (a) FESEM images of AgCl nanocrystals grown on bacterial cellulose. The concentrations of Silver Nitrate in samples (a-d) are 100 mM, 10 mM, 1 mM, 0.1 mM respectively.

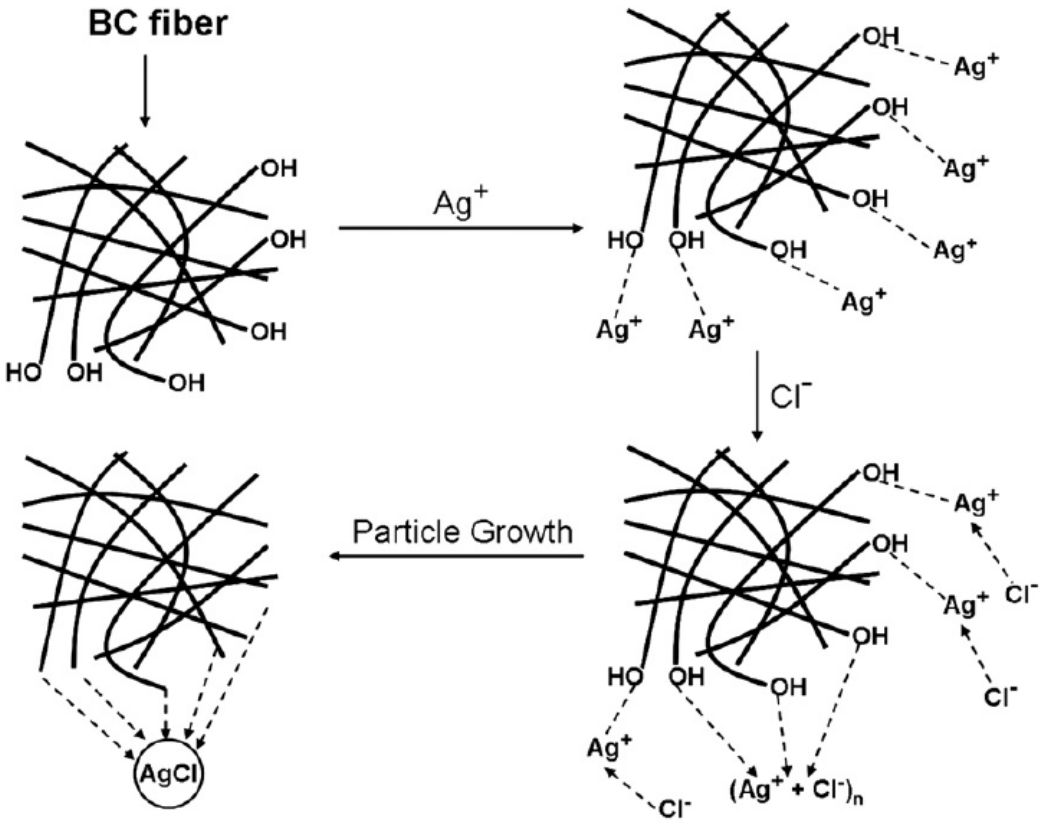

Figure 5.10 Mechanism of formation of AgCl nanocrystals[19].

X –ray diffraction method was used to determine the presence of the cubic nanocrystals. Figure 5.6 shows the XRD diffraction data of BC , AgCl incorporated BC and silver nanoparticles incorporated BC. Three peaks at 14.60°, 16.82°and 22.78° are attributed to the characteristic interplanar distances of cellulose I_α and I_β phases. In Figure 5.6(b), other characteristic peaks at 27.82°, 32.24°, 46.25°, 54.81° and 57.56° correspond to the (1,1,1), (2,0,0), (2,2,0), (3,1,1) and (2,2,2) crystal planes of AgCl[19]. In Figure 5.6(c) we see that the characteristic peaks of AgCl disappears and we see a peak at 38.35° which

corresponds to the Ag[111] peak[20]. This confirms the presence of Ag(0). The EDAX spectrum in Figure 5.5 shows the presence of silver and absence of significant chloride ion, which indicated that the reduction process has indeed reached towards conclusion.

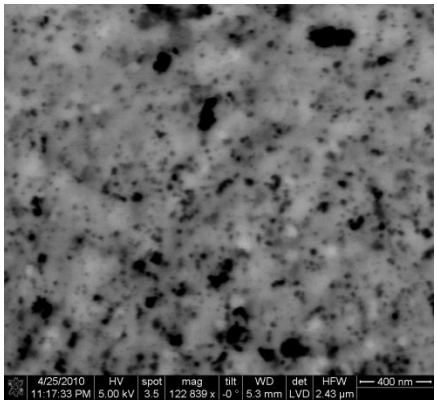

Figure 5.11 FESEM image of bacterial cellulose after reduction of AgCl by sodium sulfite/acetic acid.

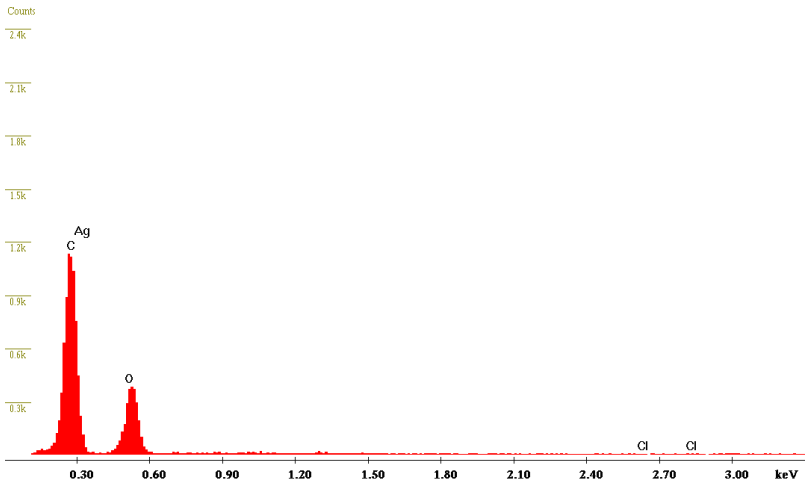

Figure 5.12 EDAX spectrum shows presence of silver in the sample where AgCl was reduced by sodium sulfite/acetic acid.

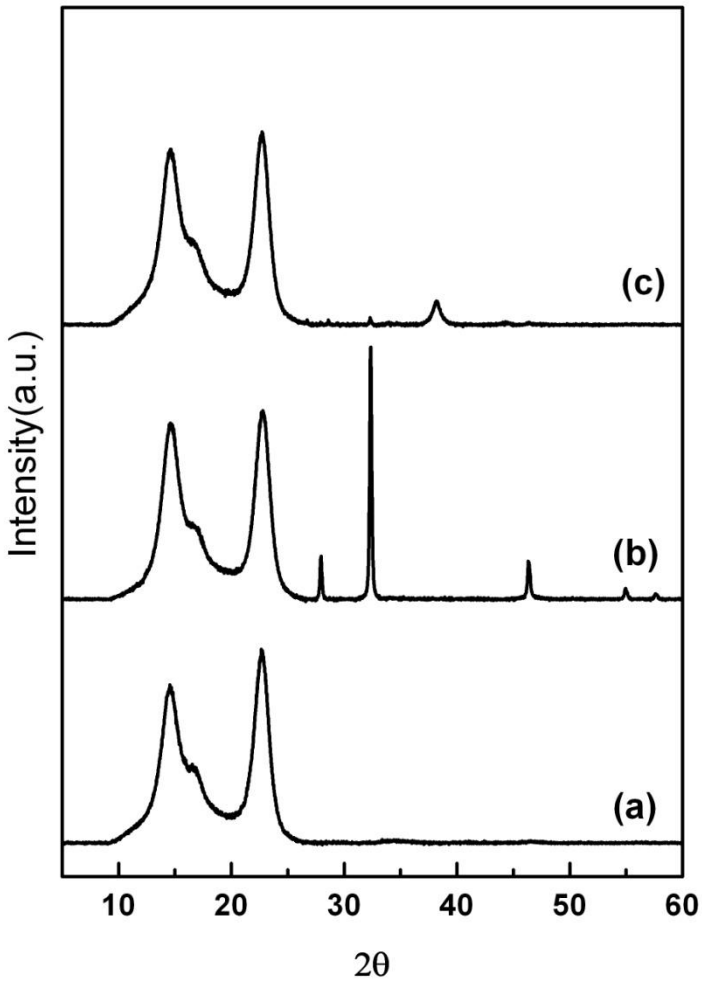

Figure 5.13 XRD spectra of (a) bacterial cellulose (BC,) (b) BC with AgCl nanocrystals, (c) BC with reduced AgCl by sodium sulfite/acetic acid.

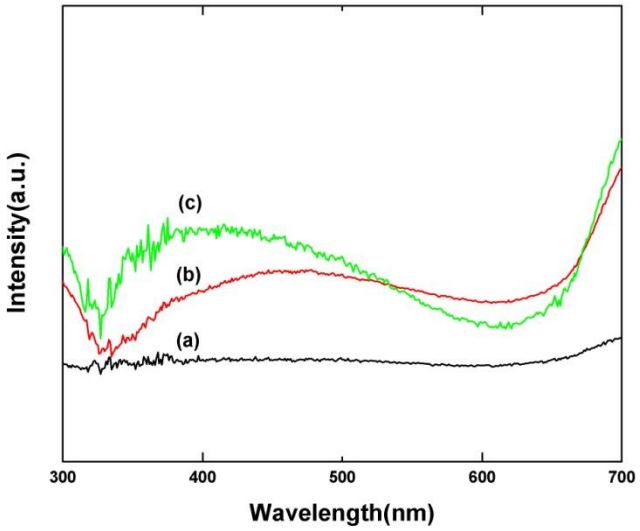

Figure 5.14 Uv-Vis spectra of (a) Bacterial cellulose (B) BC incorporated with silver nanoparticles produced by reduction by ferrous ions (c) BC incorporated with reduced AgCl.

The BC membrane have nanopores in them which allows ions to be carried into it through aqueous medium. The silver nitrate solution contains Ag^{+} ions which gets attached to the polar oxygen groups of the hydroxyl and the ether groups as shown in Figure 5.3. As it is dipped into the NaCl solution AgCl is formed which is still firmly attached to the cellulose matrix. Reduction of the AgCl in aqueous medium was carried out by Sodium sulfite in the presence of Ascorbic acid. This reaction is an example of chemical induction in which there are two reducing agents (sodium sulfite and ascorbic acid) and one oxidizing agent. One of the reducing agent acts as the inductor while the

other acts as the acceptor. Chemical induction is a phenomenon in which substance A and substance B reacts which also brings about a reaction between C and B. The first reaction is said to induce the second reaction. But in the absence of A, B and C do not react with each other. Substance A which induces the change is called inductor and substance B which is present in both the cases is called the acceptor. In our case, Ascorbic acid is the inductor, sodium sulfite is the acceptor and silver chloride is the actor. The reaction between silver chloride and ascorbic acid produces more silver in presence of sodium sulfite than its absence. The reaction goes as:

$$AH_2 + 2AgCl \rightarrow A + 2Ag + 2HCl$$
$$AH_2 \rightleftarrows A^{--} + 2H^{+}$$
$$A^{--} + 2Ag^{+} \rightarrow 2Ag + A$$

Where ascorbic acid is denoted by AH_2. From the above equations we can see that ascorbic acid undergoes dissociation. The silver ions take the electrons from the anion of the reducing agent and are reduced to metallic silver.

$$A + Na_2SO_3 + H_2O \rightarrow AH_2 + Na_2SO_4$$

The role of sodium sulfite is to regenerate the ascorbic acid from dehydroascorbic acid, which cannot reduce silver chloride.

We have used one more process of reduction of silver ions by ferrous ions in presence of acetic acid[21]. This is a simple method of reducing silver ions at ambient temperature and does not require the use of any harsh chemical reducing agents. The presence of Ag(0) was seen from the Uv-vis peak (Figure 5.7) which has a broad absorbtion peak at around 450 nm. We performed SERS using this silver nanoparticles incorporated substrate (Figure 5.8) as a demonstration for its use as a substrate for SERS. We were able to get good SERS signals of 10^{-7} M R6G on this substrate (Figure 5.9).

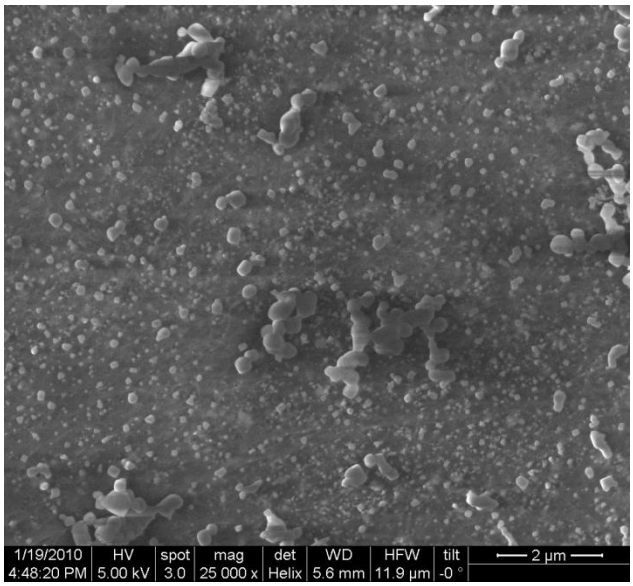

Figure 5.15 Silver nanoparticles on bacterial cellulose roduced by reduction with ferrous ions.

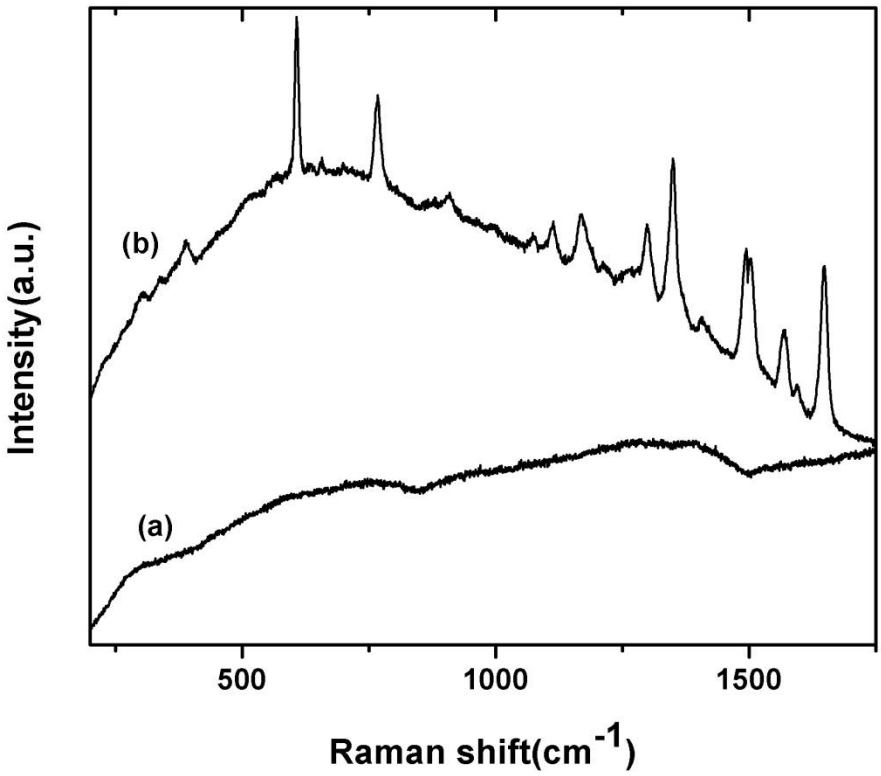

Figure 5.16 (a) Raman spectra of BC dipped in 10^{-4}M R6G solution, (b) SERS spectra of R6G on silver nanoparticle incorporated BC.

5.4 Conclusion and future work

Silver nanoparticles have been produced in the bacterial cellulose template by using environmental friendly green method of synthesis. Ascorbic, Sodium Sulfite and acetic acid are non toxic chemicals normally used in food products. Therefore reduction of silver salt using these materials is a green method to prepare potential antibacterial materials to be used in variety of purposes like wound dressing, food processing etc. Results also illustrate that the size and area coverage is also possible in this method and therefore this method will be helpful in preparing bacterial cellulose nanoparticle composite with uniform nanoparticle size and composition. We are in the process of optimizing SERS using these templates and also work is going on to control the particle sizes in a more efficient manner.

5.5 References

[1] J. J. Storhoff, C. A. Mirkin, *Chemical Reviews* **1999**, *99*, 1849.

[2] T. Torimoto, M. Yamashita, S. Kuwabata, T. Sakata, H. Mori, H. Yoneyama, *Journal of Physical Chemistry B* **1999**, *103*, 8799.

[3] A. P. Alivisatos, K. P. Johnsson, X. G. Peng, T. E. Wilson, C. J. Loweth, M. P. Bruchez, P. G. Schultz, *Nature* **1996**, *382*, 609.

[4] L. A. Gugliotti, D. L. Feldheim, B. E. Eaton, *Science* **2004**, *304*, 850.

[5] N. Ma, C. J. Dooley, S. O. Kelley, *Journal of the American Chemical Society* **2006**, *128*, 12598.

[6] J. M. Slocik, D. W. Wright, *Biomacromolecules* **2003**, *4*, 1135.

[7] A. A. Bharde, R. Y. Parikh, M. Baidakova, S. Jouen, B. Hannoyer, T. Enoki, B. L. V. Prasad, Y. S. Shouche, S. Ogale, M. Sastry, *Langmuir* **2008**, *24*, 5787.

[8] C. M. Liu, S. H. Chung, Q. L. Jin, A. Sutton, F. N. Yan, A. Hoffmann, B. K. Kay, S. D. Bader, L. Makowski, L. H. Chen, *Journal of Magnetism and Magnetic Materials* **2006**, *302*, 47.

[9] K. N. Avery, J. E. Schaak, R. E. Schaak, *Chemistry of Materials* **2009**, *21*, 2176.

[10] B. R. Peelle, E. M. Krauland, K. D. Wittrup, A. M. Belcher, *Langmuir* **2005**, *21*, 6929.

[11] V. Bansal, P. Poddar, A. Ahmad, M. Sastry, *Journal of the American Chemical Society* **2006**, *128*, 11958.

[12] S. Sotiropoulou, Y. Sierra-Sastre, S. S. Mark, C. A. Batt, *Chemistry of Materials* **2008**, *20*, 821.

[13] D. Klemm, D. Schumann, U. Udhardt, S. Marsch, *Progress in Polymer Science* **2001**, *26*, 1561.

[14] J. R. Colvin, *Nature* **1961**, *189*, 1029-&.

[15] R. J. B. Pinto, P. A. A. P. Marques, C. P. Neto, T. Trindade, S. Daina, P. Sadocco, *Acta Biomaterialia* **2009**, *5*, 2279.

[16] D. S. dos Santos, P. J. G. Goulet, N. P. W. Pieczonka, O. N. Oliveira, R. F. Aroca, *Langmuir* **2004**, *20*, 10273.

[17] C. NARAYANA, India Patent, **2009**.

[18] K. V. Ramana, A. Tomar, L. Singh, *World Journal of Microbiology & Biotechnology* **2000**, *16*, 245.

[19] W. L. Hu, S. Y. Chen, X. Li, S. A. K. Shi, W. Shen, X. Zhang, H. P. Wang, *Materials Science & Engineering C-Biomimetic and Supramolecular Systems* **2009**, *29*, 1216.

[20] N. E. Kotel'nikova, G. Wegener, T. Paakkari, R. Serimaa, V. N. Demidov, A. S. Serebriakov, A. V. Schukarev, A. V. Gribanov, *Russian Journal of General Chemistry* **2003**, *73*, 418.

[21] B. Krishna, S. Ghosh, *The Journal of Physical Chemistry* **1951**, *55*, 1503.

Future scope

This is the age of miniaturization and in the current trend of nanodiagnostics, there is a rush to develop handheld devices which are easy to manufacture, time and cost effective, and are attractive to use. In this context, the sensitivity and the simplicity of Raman based detection techniques offers an interesting possibility as a simplified and portable diagnostive technique, which is not only cheap and easy to use but also very efficient. Already there are portable and high-resolution Raman spectrometers in the market, which makes this possible. Alongside the development of microfluidics and clubbing it with Raman provides us with an exciting area for nanodiagnostics. The ability to work with really small amounts of analyte in a controlled fashion on a chip and the added high sensitivity of Raman can help in building of technologically effective devices.

In this thesis, we have made attempts to produce possible new nano-substrates for use as a template or in solution for Raman based diagnostics. The earlier works carried out in laboratory has demonstrated the potential of clubbing both Surface Enhanced Raman Spectroscopy (SERS) and normal molecular biology in detection of DNA or RNA of pathogens without Polymerase Chain Reaction (PCR) amplification. The present thesis has been a step forward in this direction. We have synthesized nanoparticles and substrates to overcome the pitfalls of the previous developments. To illustrate this, we have developed paramagnetic core-shell nanoparticles, which have both plasmonic as well as magnetic property. The advantages of these nanoparticles are that they can be used in solution and they circumvent the difficult of washing cycles in DNA/RNA

detection. Another development has been the use of cellulose to embed the SERS active nanoparticles, which could be a very good replacement for the glass substrates. Direct immobilization of bio-molecule on cellulose helps in removing the usual difficulties in glass based kits. We have also developed graphene as a possible substrate for trace detection of biological molecules using the ‘d’-band of the graphene.

These developments though are significant are not still in the realm of technology. One of the biggest challenges is to make these techniques move from specialist to clinicians. For this, we need to make SERS as simple and as quantitative as fluorescence. This would require a lot of development. One of the immediate challenges is to improve the signal-to-noise (S/N) ratio. We are in the process to do these by tailoring the detector molecule or by “FRET” type interactions for SERS applications. The other challenge is to quantify these results to give a clinician a reliable pathogen level for effective treatment. For this, the use of intensifiers and nano-fluidics is important. A great deal of development is to be made both in photonics as well as nano-fluidics to produce these results. Preliminary investigations are positive and show great promise.